Multidecadal variability of atmospheric methane, 1000–1800 C.E.

Logan E. Mitchell,[1] Edward J. Brook,[1] Todd Sowers,[2] J. R. McConnell,[3] and Kendrick Taylor[3]

Received 2 June 2010; revised 27 January 2011; accepted 8 February 2011; published 28 April 2011.

[1] We present a new high-precision, high-resolution record of atmospheric methane from the West Antarctic Ice Sheet (WAIS) Divide ice core covering 1000–1800 C.E., a time period known as the late preindustrial Holocene (LPIH). The results are consistent with previous measurements from the Law Dome ice core, the only other high-resolution record of methane for this time period, and confirm most of the observed variability. Multidecadal variability in methane concentrations throughout the LPIH is weakly correlated or uncorrelated with reconstructions of temperature and precipitation from a variety of geographic regions. Correlations with temperature are dominated by changes in Northern Hemisphere high latitude temperatures between 1400 and 1600 C.E. during the onset of the Little Ice Age. Times of war and plague when large population losses could have reduced anthropogenic emissions are coincident with short periods of decreasing global methane concentrations.

Citation: Mitchell, L. E., E. J. Brook, T. Sowers, J. R. McConnell, and K. Taylor (2011), Multidecadal variability of atmospheric methane, 1000–1800 C.E., *J. Geophys. Res.*, *116*, G02007, doi:10.1029/2010JG001441.

1. Introduction

[2] Atmospheric methane, the second most important greenhouse gas directly impacted by anthropogenic activities, accounts for 18% of the total increase in radiative forcing by all long-lived greenhouse gases and varied in the past on timescales ranging from seasons to hundreds of thousands of years [e.g., *Bousquet et al.*, 2006; *Forster et al.*, 2007; *Loulergue et al.*, 2008]. Systematic direct atmospheric measurements since 1983 from the NOAA (E. J. Dlugokencky et al., Atmospheric methane dry air mole fractions from the NOAA ESRL Carbon Cycle Cooperative Global Air Sampling Network, 1983–2009, Version 2010-08-12, 2010, available at ftp://ftp.cmdl.noaa.gov/ccg/ch4/flask/event/) and GAGE/AGAGE [*Cunnold et al.*, 2002] sampling networks reveal that methane sources and sinks are perturbed by seasonal climate cycles, atmospheric chemistry, large-scale atmospheric patterns such as El Niño Sothern Oscillation (ENSO), volcanic eruptions, and anthropogenic activities [*Bousquet et al.*, 2006; *Steele et al.*, 1987]. These direct measurements also documented a surprising decrease in the methane growth rate during the 1990s and a recent resumption of growth [*Dlugokencky et al.*, 2009]. Understanding methane variability on decadal to multidecadal timescales and discriminating between changes in natural and anthropogenic sources is difficult because of spatial and temporal variability of sources and sinks. Furthermore, direct atmospheric records are not yet long enough to assess variability on multidecadal timescales and ice core records have rarely achieved the precision and time resolution needed to observe changes on such short timescales. These limitations have made it difficult to place the decadal-scale variability observed in the record of direct atmospheric measurements in a longer term context.

[3] Air occluded in polar ice sheets provides a unique archive that enables us to extend our record of methane into the past. Accumulation rate (i.e., annual accumulation of snowfall) is one of the primary factors that limit the temporal resolution of ice core paleoatmospheric reconstructions. Long records from low accumulation sites (≤50 kg m^{-2} yr^{-1}) such as Vostok and Dome C have revealed orbital-scale variability over the last 800,000 years [e.g., *Delmotte et al.*, 2004; *Loulergue et al.*, 2008] but do not preserve the detail needed to examine short-term variability because diffusion in the firn smoothes the records [*Spahni et al.*, 2003]. The degree of smoothing is much smaller at sites where accumulation rates are high, and the most detailed history of methane over the last few millennia is captured in ice cores from Law Dome in East Antarctica [*Etheridge et al.*, 1998; *MacFarling Meure et al.*, 2006], where the very high accumulation rate (600–1100 kg m^{-2} yr^{-1}) allows for large sample sizes yielding precise measurements, high temporal resolution, and excellent chronological control. Furthermore, the Law Dome ice core and firn air records overlap with direct atmospheric measurements and confirm that polar ice faithfully preserves past atmospheric concentrations of methane.

[1]Department of Geosciences, Oregon State University, Corvallis, Oregon, USA.
[2]Earth and Environmental Systems Institute, Pennsylvania State University, University Park, Pennsylvania, USA.
[3]Desert Research Institute, Nevada System of Higher Education, Reno, Nevada, USA.

0148-0227/11/2010JG001441

[4] In this study we present a new, precise, decadally resolved ice core methane record spanning 1000–1800 C.E., a period known as the late preindustrial Holocene (LPIH) [*Etheridge et al.*, 1998]. The results come from the West Antarctic Ice Sheet (WAIS) Divide ice core site (core WDC05A). We confirm the magnitude and timing of multidecadal variability observed in the Law Dome methane record over this time period. We also investigate correlations between our methane concentration record and paleoclimate and historical records relevant to methane sources to investigate the processes which likely controlled LPIH methane variations.

2. Methods

2.1. WDC05A Core Recovery

[5] A deep ice core, the WAIS Divide Core (WDC), is located on the West Antarctic Ice Sheet divide at 79.467°S, 112.085°W, surface elevation of 1759 m. The modern annual accumulation rate of ~200 ± 34 kg m^{-2} yr^{-1}[*Banta et al.*, 2008], mean temperature of −31°C, and the simple ice flow regime at the site are ideal for high-resolution analysis of greenhouse gases over the past ~110,000 years [*Morse et al.*, 2002]. These characteristics are similar to high-resolution deep ice cores in central Greenland (GISP2, GRIP, and NGRIP) simplifying interhemispheric comparisons. The samples used here came from a 298 m shallow core that was extracted in the austral summer of 2005/2006 (WDC05A) 1.3 km northwest of the main borehole (WDC06A). It was drilled with a 10 cm electromechanical drill without drilling fluid and core quality was excellent.

2.2. Analytical Procedures

2.2.1. Methane Measurements

[6] Samples were processed using a wet extraction technique similar to that described by *Grachev et al.* [2007, 2009] and further elaborated on here. The outer 1–2 mm of ice samples was removed with a band saw in a −25°C freezer to produce fresh ice that was not recently exposed to the modern atmosphere. This ice was divided in half along the vertical axis to produce a pair of samples with the same depth and age. Each sample had a cross-sectional area of ~2.5 cm^2, height of ~10 cm, and weight of 50–63g. Samples were weighed to the nearest 0.1 g and placed in precooled cylindrical glass vacuum flasks joined to stainless steel CF flanges with a glass to metal transition, manufactured by Larson Electronic Glass (Redwood City, CA, USA). Each flask was bolted to a stainless steel vacuum line assembly and sealed with a copper O-ring. Valves on the vacuum line are pneumatically actuated Swagelok bellows sealed valves with Polychlorotrifluoroethylene (PCTFE) stem tips. The vacuum line accommodated eight flasks. The flasks were submerged in an ethanol bath maintained at −60°C to −70°C and ambient air was removed by pumping with a turbo molecular pump (Alcatel ATP80) backed with a dry (scroll) pump for 1 h. The valves to the flasks were then closed and flasks were submerged in a warm water bath at ~50°C to completely melt the ice and release the gas into the headspace above the water. Melting was usually complete in ~15 min. The flasks were then resubmerged in the ethanol bath for 1 h to freeze the samples and prevent water vapor from interfering with the measurements. The air in the headspace of the flasks was expanded to a 10 cm^3 sample loop on a six-port Valco gas sampling valve. Samples were injected on to a packed column (6 foot, 1/8 inch Hayesep D 80/100 mesh) in an Agilent Technologies 6890N Gas Chromatograph (GC) equipped with a flame ionization detector, using ultrapure nitrogen as a carrier gas. The pressure in the sample loop was measured using an MKS Baratron capacitance manometer (0–100 torr, 0.15% accuracy) installed in the GC oven for temperature stability. The air from each sample was analyzed four times with the pressure of the first expansion ($P_{\mathrm{Headspace}}$) typically between 35 and 45 torr and the last 10–20 torr. The peak area over loop pressure ratio was measured for each air sample and compared to a linear regression line fitted to the ratios from a working air standard (500.22 ppb methane on the NOAA04 methane scale [*Dlugokencky et al.*, 2005]) covering the entire range of sample pressures. Concentrations from the four measurements from each sample were then averaged to produce a mean methane concentration for each sample. Mean concentrations were averaged for each pair of samples to produce a mean concentration for each depth/age (Figure 1).

[7] Calibration of daily measurements was maintained throughout the experiment by analyzing our working air standard tank 12 times each day over the pressure range of 10–50 torr. The working air standard tank was a high-pressure cylinder of synthetic air prepared by Scott-Marrin Inc. that was calibrated to primary laboratory standard tanks with concentrations ranging from 380 to 1853 ppb, which were calibrated by the NOAA GMD Carbon Cycle Group on the NOAA04 methane scale [*Dlugokencky et al.*, 2005]. The response of the measurement system is linear to better than 1.5 ppb over the standard tank concentration range. This implies a negligible correction over the sample concentration range so we have assumed a linear response.

[8] Over the course of this study 294 samples from 147 depths were measured. The results from two depths were rejected due to leaks. In addition, we further investigated the 5% of samples (7 depths) with the greatest disagreement between the sample pairs (>5.9 ppb). We measured additional duplicate samples from the same or adjacent depths and in the three depths with the greatest disagreement (10.5–11.8 ppb) we observed that of the four samples measured there was good agreement between three of them and one outlier. In these three cases we suspected that the outlier was a result of contamination or a leak and rejected that pair of samples. Between 21 September and 23 October 2007 we noticed slightly higher methane levels than expected in 34 samples, and traced the contamination to a change in flask cleaning procedures after a personnel change. We detected this contamination when measurement of air-free ice (see below) indicated a contamination of 5–14 ppb. To eliminate the contamination, we cleaned the flasks daily (i.e., after every use) with Alconox® detergent soap, whereas prior to 23 October we had cleaned the flasks weekly. Additional samples from identical or adjacent depths to the contaminated samples were measured after daily cleaning of flasks was implemented. Duplicate measurement of the samples analyzed prior to 21 September and after 23 October 2007 yielded consistent results. All results, including leaks, outliers, and contaminated samples, are shown in Figure 1.

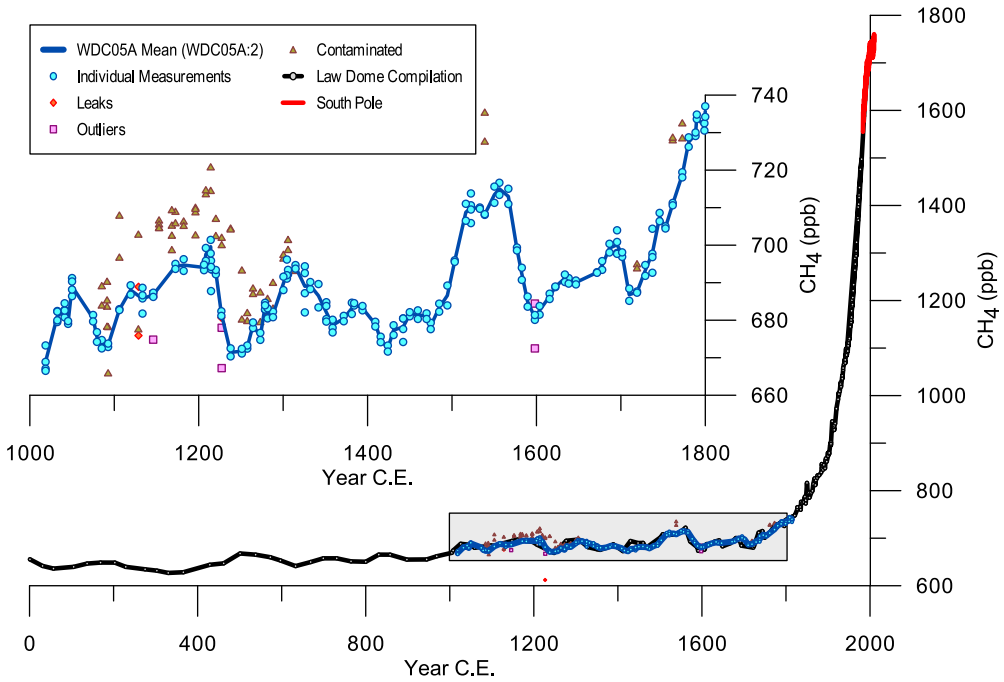

Figure 1. Atmospheric methane concentrations over the past 2 centuries from the Law Dome compilation (0–1995 C.E., black line) [*Etheridge et al.*, 1998; *MacFarling Meure et al.*, 2006], WDC05A on the WDC05A:2 chronology (1019–1814 C.E., blue line), and direct atmospheric measurements from the South Pole (1983–2010 C.E., red line) (E. J. Dlugokencky et al. Atmospheric methane dry air mole fractions from the NOAA ESRL Carbon Cycle Cooperative Global Air Sampling Network, 1983–2006, version 2007-09-19, report, 2007). Inset shows methane data from WDC05A on the WDC05A:2 chronology with the mean at each depth/age (blue line), individual measurements (light blue circles), leaks (red diamonds), outliers (pink squares), and contaminated measurements (brown triangles). All data are plotted on the NOAA04 calibration scale [*Dlugokencky et al.*, 2005].

[9] The average standard error of the four analyses for individual samples was 1.4 ppb and the pooled standard deviation between the means of the sample pairs was 1.9 ppb. These statistics exclude the rejected results described above. To quantify the long-term reproducibility of the methane analysis, we measured 16 duplicate pairs of ice samples with the time between measurements ranging from days to months. These duplicates had the same depths as the original samples and should therefore have identical methane concentrations. The pooled standard deviation between the mean of the original and duplicate pairs of samples is 2.8 ppb which is the value we use to represent the long-term analytical uncertainty (1σ) for this data set. The greater variability observed in these duplicates most likely comes from subtle changes in the solubility of gases in the meltwater, discussed in greater detail below.

2.2.2. Corrections to Measurements

2.2.2.1. Blanks

[10] To constrain the influence of leaks or other contamination in our analysis line, we routinely measured air-free ice (AFI). To create AFI, we boiled ultrapure, 18 MΩ water in a cylindrical stainless steel vacuum flask with a Conflat flange seal and metal bellows seal valve welded to the top flange. We affixed a ~30 cm piece of 1/8 inch stainless steel tubing to the outlet, and during boiling the valve remained open. The boiling drives air from the water, which is swept from the chamber by the released steam. We boiled the water for 30 min then sealed the bellows and slowly froze the remaining liquid from the bottom up in an ethanol bath kept at −20°C. Sample preparation and analysis of the artificial ice was identical to ice core samples with the exception that before the artificial ice was melted in the flasks, sufficient standard air from our working air standard tank was added to the flasks so that when expanded to the sample loop it produced pressures equivalent to those from ice core samples. In this way any errors resulting from leaks or contamination of the flasks could be quantified and corrected for. Average AFI corrections were linearly interpolated between days when AFI was analyzed to create a time-dependent correction to the data. The average AFI correction was 1.1 ± 0.5 (1σ) ppb.

2.2.2.2. Solubility of Methane in Water

[11] Gases dissolve in liquid water with the partitioning between the air and water described by Henry's law. Methane is ~2.5X as soluble as nitrogen and therefore the headspace methane concentration decreases when air is exposed to liquid water. As the water is refrozen a small fraction of the air is trapped in the ice leading to a depletion of methane in the headspace after freezing. We express a methane solubility correction factor as

$$\text{Correction Factor} = \frac{[CH_4]_{\text{Total}}}{[CH_4]_{\text{Headspace}}} \quad (1)$$

where $[CH_4]_{Headspace}$ is the concentration in the headspace which we measure during our typical analysis and $[CH_4]_{Total}$ can be expressed as the molar ratio

$$[CH_4]_{Total} = \frac{\{CH_4\}_{Headspace+Water}}{\{Ar + O_2 + N_2 + CH_4\}_{Headspace+Water}} \quad (2)$$

where $\{CH_4\}_{Headspace+Water}$ and $\{Ar + O_2 + N_2 + CH_4\}_{Headspace+Water}$ are the total number of moles that were in the original ice sample. Inclusion of trace atmospheric gases has a negligible effect and was ignored. At equilibrium the distribution of air constituents between the headspace and the meltwater is dictated by Henry's law constants at 273.2 K [*Fogg and Sangster*, 2003] because the majority of dissolution happens as bubbles escape from the melting ice sample and rise through the meltwater next to it. Using typical values for flask and ice volumes, the headspace air would have a methane concentration depleted by 2.1–2.2% relative to the original concentration. For example, a sample which has a measured $[CH_4]_{Headspace}$ of 700 ppb, 60 mL of water in a 134 cm^3 flask, at 273.2 K, would have a $[CH_4]_{Total}$ of 715 ppb and therefore a correction factor of 1.021.

[12] We examined this correction factor empirically by measuring the concentration of methane in the frozen sample water ($[CH_4]_{Refreeze}$) after our typical analysis was completed for 32 samples. After the initial melt-refreeze-CH_4 measurement was completed we evacuated the headspace for 1 h then another melt-refreeze-CH_4 measurement was done. $[CH_4]_{Total}$ was then calculated as follows:

$$[CH_4]_{Total} = \frac{[CH_4]_{Headspace}P_{Headspace} + [CH_4]_{Refreeze}P_{Refreeze}}{P_{Headspace} + P_{Refreeze}} \quad (3)$$

where P is pressure in torr. Mean and standard deviations (1σ) from the 32 measurements were $P_{Refreeze} = 0.50 \pm 0.06$ torr and $[CH_4]_{Refreeze} = 1698 \pm 169$ ppb. The correction factor from these experiments is therefore $1.0170 \pm 0.0031\%$. Since $P_{Refreeze}$ is ~1% of $P_{Headspace}$, we expect the amount gas trapped in the ice during the second melt-refreeze cycle to be ~1% of $P_{Refreeze}$, or ~0.005 torr, and therefore negligible.

[13] The uncertainty in the correction factor is probably caused by a variety of subtle differences between samples such as sample size, air content, and the refreezing rate. This uncertainty is inherently incorporated into our estimate of the long-term uncertainty of our measurements because it is derived from duplicate measurements from different days and should therefore represent the full range of possible variability. Given these considerations we have increased our final methane concentration values by the average empirically derived solubility correction factor of 1.0170.

[14] The difference between the calculated and empirical correction factors is likely caused by the headspace air not reaching a solubility equilibrium with the meltwater when the samples are refrozen. This has been observed in greater detail in other studies with much larger samples [*Petrenko et al.*, 2008]. The values given above indicate that the samples reach ~80% of solubility equilibrium, presumably because of exclusion of gases during freezing. Slower refreezing may reduce the effect at the expense of longer processing times.

2.2.2.3. Gravitational Fractionation

[15] Gases within the firn undergo mass dependant fractionation due to gravity [*Craig et al.*, 1988; *Schwander*, 1989; *Schwander et al.*, 1997; *Sowers et al.*, 1989]. The magnitude of gravitational fractionation is controlled by the thickness of the diffusive air column in the firn and can be estimated by measuring the $^{15}N/^{14}N$ ratio of N_2 and reported using standard delta notation as $\delta^{15}N_2$. Because the turnover time of the atmospheric N_2 reservoir is longer than a million years, we can assume that the $^{15}N/^{14}N$ ratio of atmospheric N_2 has remained constant over ice core timescales [*Sowers et al.*, 1992]. Measurement of $\delta^{15}N_2$ along the main core (WDC06A) at WAIS Divide (100–300 m) revealed $\delta^{15}N$ values of 0.303 ± 0.006‰ (J. Severinghaus, personal communication, 2010). Gravitational fractionation of methane concentrations results from the mass difference between methane (M = 16.04 g mol^{-1}) and dry air (M = 28.96 g mol^{-1}). The gravitational correction is therefore $\Delta M \times \delta^{15}N_2$ where ΔM = 12.92 g mol^{-1}. This results in a gravitational fractionation correction (increase of the measured concentration) of 0.39% which we have applied to all of our ice core measurements. The $\delta^{15}N_2$ is not expected to be significantly different between the WDC05A and WDC06A cores.

2.3. WDC05A Chronology

[16] Convective and diffusive processes move air through the firn faster than the annual accumulation of ice causing air to be younger than the surrounding ice at a given depth within the firn [*Schwander*, 1989]. The age difference between the air and the enclosing ice is termed "delta age" (Δage). The original WDC05A chronology [*Mischler et al.*, 2009], was based on annual layer counting of the non-sea-salt sulfur to sodium ratio (nssS/Na) between the surface and 70 m [*Banta et al.*, 2008] and alternative current electric conductivity measurement (ACECM) measurements from 70 to 298 m to establish the age of the ice. A 1-D firn air diffusion model following *Battle et al.* [1996] and *Trudinger et al.* [1997] was used to estimate the mean age of the air at the lock in depth (LID) which is then subtracted from the age of the ice at the LID to estimate Δage [*Mischler et al.*, 2009]. The ice chronology from 70 to 298 m was recently improved by optimizing correlations between the monthly resolved mineral acidity measurements from the main borehole (WDC06A) which are dominated by fallout from volcanic emissions and the WDC05A ACECM measurements. Annual layer counting of the high-resolution chemical records from the upper 70 m of WDC05A and WDC06A from ~1300 C.E. to ~2000 C.E. was confirmed by comparison with the volcanic sequence of nssS from Law Dome, adapted from *Palmer et al.* [2001]. This generated 71 unique tie points between the WDC05A and WDC06A records. The annual accumulation rate from WDC06A was then mapped onto WDC05A assuming a linear change between tie points. To evaluate the uncertainty in the estimated ice age for WDC05A, we compared the estimated ice ages in the upper 70 m with those determined from high-resolution chemistry measurements on the same core. For the 231 years common to both records, the average difference between the two depth-age scales is 0.056 m_{weq} (water equivalent), with a maximum difference of 0.283 m_{weq}. The mean annual accumulation rate is ~0.20 m_{weq}, so the mean difference is 3–4 months. The maximum difference corresponds to

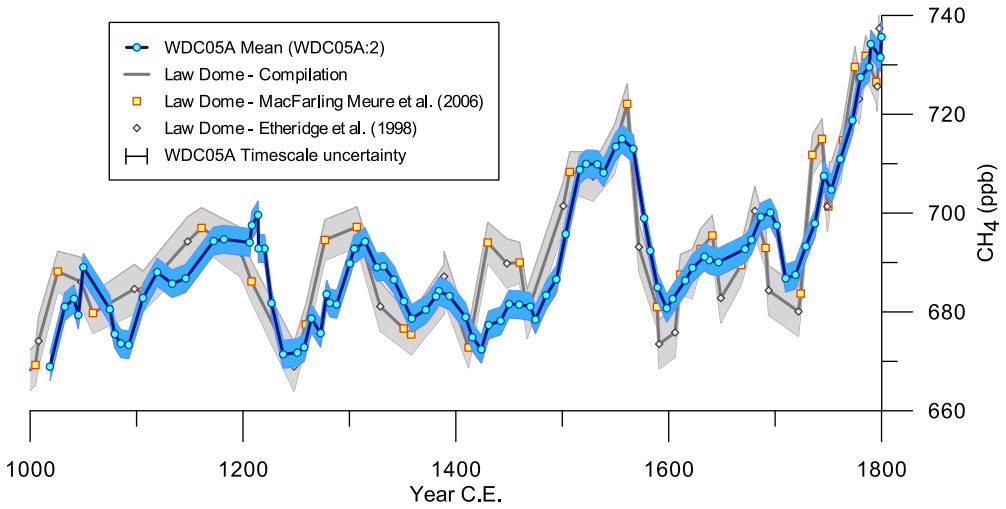

Figure 2. Comparison between the WDC05A (mean values) on the WDC05A:2 chronology and Law Dome methane records. Error bands are ±2.9 ppb for WDC05A, ±5 ppb from *Etheridge et al.* [1998], and ±4.1 ppb from *MacFarling Meure et al.* [2006]. All records are plotted on the NOAA04 calibration scale [*Dlugokencky et al.*, 2005]. Chronology uncertainty for WDC05A is ±10 years.

~1.4 years and the standard deviation between the estimated and observed depth-age scales is ~0.07 m_{weq} or ~4 months. The difference between our final ice chronology (WDC05A:2) and the original ice chronology (WDC05A:1) [*Mischler et al.*, 2009] is negligible between 0 and 70 m, increasing to 13 years at 148 m, and then decreasing to −36 years at 298 m.

[17] A visible volcanic ash layer observed in both cores was also used to confirm the dating of the two cores. The ~5 mm volcanic ash layer was observed at 190.83 m (1248.1 C.E.) in WDC05A and 190.39m (1248.5 C.E.) in WDC06A (ages determined using the revised chronologies). Electron microprobe analysis indicates that the chemical composition, grain size and particle morphology of the two layers are nearly indistinguishable, indicating that both are from the same eruption and therefore deposited contemporaneously (N. Dunbar, personal communication, 2010). The ash layer has abundant ash particles and is relatively coarse grained with particles up to 20 μm suggesting that it has an Antarctic source. Positive chemical correlations with ash layers in the Siple Dome and Taylor Dome ice cores indicate that this ash layer is a major regional time stratigraphic marker [*Dunbar et al.*, 2003, 2007].

[18] A 1-D firn air diffusion model estimated that the mean age of the air within the open porosity at the LID (65.5 m at WDC05A) is 9.9 years for CO_2 and 7.2 years for CH_4 (M. Battle, personal communication, 2009). The difference between the mean age of CH_4 and CO_2 arises from the different diffusivities of the two gases in the firn air. The width of the CH_4 age distribution at half height is 5.9 years. The age of the ice at the LID is 215 years which makes Δage 205.1 years for CO_2 and 207.8 years for CH_4. Since temperature (E. Steig, personal communication, 2010) and accumulation at WDC05A have remained relatively constant in the LPIH we do not expect that Δage has changed significantly and for the purpose of creating a chronology have held it constant. To construct the final gas chronology, we have subtracted 207.8 years from the ice chronology. The estimated uncertainty of the chronology is ± 10 years based on a detailed comparison between our record and the Law Dome methane record, discussed below. This chronology is designated WDC05A:2.

3. Results and Discussion

3.1. Comparison With Previous High-Resolution Antarctic Data From Law Dome

[19] Replication of paleoclimate records is an important means of verifying their reliability. The methane record from Law Dome, Antarctica, a well-known data set covering the last 2000 years, is a compilation of data from three different ice cores (DSS, DE08, DE08–2) and until now has been the only high-resolution, high-precision record covering the past 1000 years [*Etheridge et al.*, 1998; *MacFarling Meure et al.*, 2006]. The Law Dome record from 1000 to 1800 C.E. comes from the DSS ice core and the data are plotted with the WDC05A results in Figure 2, after conversion of Law Dome results to the NOAA04 calibration scale [*Dlugokencky et al.*, 2005]. Error bands are ± 2.8 ppb for WDC05A, ± 5 ppb for DSS samples reported by *Etheridge et al.* [1998], and ± 4.1 ppb for DSS samples reported by *MacFarling Meure et al.* [2006]. The Law Dome data were produced using a dry extraction technique with large samples (500–1500g) while we use a wet extraction technique with small samples (two samples, ~60 g each) which requires a correction for solubility effects (discussed above).

[20] Law Dome is located at 66.733°S, 112.833°E, with a surface elevation of 1390 m and is over 3500 km away from the WAIS Divide site. Since there are essentially no sources of methane in the high latitude Southern Hemisphere, the atmospheric concentration around Antarctica is homogenous [*Dlugokencky et al.*, 1994] and should have been so in the past. The absolute methane concentrations in both records are very consistent (Figure 2). The only time interval where the records differ beyond the 1-σ envelope of analytical and temporal uncertainty is 1410–1470 C.E. where they diverge by 10–15 ppb. This is within the 2-σ level and despite the

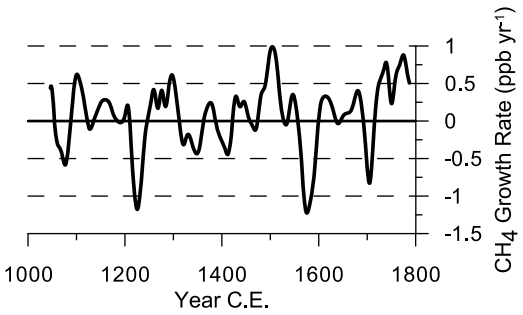

Figure 3. Methane growth rate computed numerically after linear interpolation between WDC05A data points then smoothed with a 30 year Gaussian filter.

divergence both records show a peak in concentrations during this time period. We observe that the amplitude of high-precision variability in the WDC05A core is ~10–20% smaller than in Law Dome. The exact mechanisms behind the slight amplitude reduction are not currently known but we speculate that it is a result of greater mixing of air within the lock in zone during the bubble closure process, which is longer at WDC05A because of the lower accumulation rate.

[21] The data from WDC05A and Law Dome show that atmospheric methane in the high latitude southern hemisphere averaged ~690 ppb (NOAA04 scale) and experienced multidecadal variability during the LPIH. During the 18th century anthropogenic activities increased methane emissions and caused global concentrations to increase rapidly [*Etheridge et al.*, 1998; *MacFarling Meure et al.*, 2006]. The general trends in methane concentration during the 19th and 20th centuries have been described in greater detail elsewhere and preliminary measurements from WDC05A (not shown) support those previous conclusions [*Etheridge et al.*, 1998; *MacFarling Meure et al.*, 2006]. Here we focus on a detailed comparison with previously published high-resolution records of methane during the LPIH.

[22] A statistical comparison of the two methane records shows a high degree of correlation (r = 0.87 for linear regression). The WDC05A record appears to slightly lag the Law Dome record. A maximum correlation (r = 0.91) between the records is obtained by shifting the WDC05A record 9 years older. While it is not possible to determine which record is "correct," the highest correlation occurs within the stated uncertainty of ± 10 years for the WDC05A gas chronology [*Mischler et al.*, 2009], which is largely due to uncertainty in Δage. One possible explanation for the offset is that the firn air model used by *Mischler et al.* [2009] to deduce Δage for WDC05A assumes that all bubbles close off below the Lock in Depth (LID). This assumption has been used in the past for sites with a similar temperature and accumulation rate as WAIS Divide such as Summit, Greenland but observations suggest that as much as 20% of the bubbles close above the LID [*Schwander et al.*, 1993]. Gradual bubble closure was included in the firn air transport model used for the Law Dome ice cores, but the large accumulation rate at this site reduces the magnitude of this effect [*Trudinger et al.*, 1997]. Qualitatively, bubble closure above the LID combined with a low to moderate accumulation rate would decrease Δage and cause additional smoothing of the gas records, consistent with our observations.

[23] Alignment of large rapid changes in methane concentrations have been used to establish chronostratigraphic tie points between ice cores in the past because methane has a relatively short lifetime and variations recorded in polar ice cores are expected to represent global signals [*Blunier and Brook*, 2001; *Brook et al.*, 2005; *EPICA Community Members*, 2006; *Lemieux-Dudon et al.*, 2010]. This approach has generally not yet been utilized for small-scale variations (≤50 ppb) because methane records have, until now, lacked sufficient temporal resolution and analytical precision to uniquely identify small-scale variability. The high degree of correlation between the Law Dome and WDC05A methane records demonstrate that this technique could be a viable way to establish chronostratigraphic tie points between high-precision methane records from moderate to high accumulation rates.

3.2. Multidecadal Methane Variability From 1000 to 1800 C.E.

3.2.1. Implications for the Global Methane Budget

[24] The global methane budget can be expressed in its simplest form as $dB/dt = S - B/\tau$, where B is the total atmospheric burden (Tg of CH_4), S is the total source in Tg yr^{-1}, and τ is the lifetime of CH_4 in years. The average LPIH methane concentration from WDC05A is ~690 ppb and the interpolar gradient is 43 ± 5 ppb based on preliminary measurements from the Greenland ice core GISP2D (not shown) [*Mitchell and Brook*, 2009]. The global mean atmospheric concentration, weighted by surface area, has been estimated for the LPIH as the Antarctic concentration plus 37% of the interpolar gradient [*Etheridge et al.*, 1998] and is therefore ~706 ppb from our data. Using the total mass of the dry atmosphere ($5.1352 \pm 0.0003 \times 10^{18}$ kg [*Trenberth and Smith*, 2005]) the global average atmospheric burden is calculated to be ~2008 Tg (2.844 Tg CH_4 ppb^{-1}) for the LPIH at steady state ($dB/dt = 0$). Numerous chemical modeling studies have tried to determine likely values for S and τ for the LPIH, but these are sensitive to the concentration of OH, the primary sink for CH_4, and its interaction with the CH_4-CO-NO_X chemical system. These models have produced estimates of LPIH τ that range from 17% lower to 16% higher than the present-day range of 8.9–9.2 years [*Dentener et al.*, 2003; *Harder et al.*, 2007; *Martinerie et al.*, 1995; *Prinn et al.*, 2001; *Shindell et al.*, 2003]. For the purposes of the discussion here we choose a LPIH τ of 8 years, implying a steady state flux of ~250 Tg CH_4 yr^{-1}.

[25] We estimated the methane growth rate by linearly interpolating the WDC05A data annually, then determining the annual rate of change. This time series was smoothed with a 30 year Gaussian filter (Figure 3). The most negative growth rates occurred in the early 13th and late 16th centuries while the most positive growth rates occurred at the turn of the 16th century. The interannual variability of methane growth rates may have been greater given that the modern record of direct atmospheric measurements since 1983 record which shows variations of up to ± 15 ppb CH_4 yr^{-1} [*Bousquet et al.*, 2006; *Dlugokencky et al.*, 2009], but such short-term changes would not be captured by the ice core record. The overall decrease of ~10 ppb yr^{-1} over this

Table 1. LPIH Methane Sources[a]

Global Methane Sources	Methane (Tg CH_4 yr^{-1})	Percent of Total
Animals	18.0	7.2
Termites	19.2	7.7
Ocean	12.9	5.2
Fresh water lakes	4.8	1.9
Misc ground	6.8	2.7
Biomass burning	3.8	1.5
Wetlands and tundra	155.8	62.3
Anthropogenic	28.6	11.5
Total	250	100

[a]LPIH methane sources are after *Harder et al.* [2007] with the estimate of anthropogenic source after *Houweling et al.* [2000]; scaled to a total of 250 Tg CH_4 yr^{-1}. See Table 3 for alternate estimates of anthropogenic sources.

time period [*Dlugokencky et al.*, 2009] is, however, sustained for long enough that similar changes in the past would have been preserved in the ice core record after smoothing of the firn at the WAIS Divide site. This recent change in the growth rate is therefore larger than any we observe during the LPIH.

[26] It has been common in the ice core literature to interpret past variations as indicators of changes in climate driven methane sources, primarily wetlands, although most work has recognized the possibility that the methane sink can change [*Fischer et al.*, 2008; *Kaplan et al.*, 2006; *Valdes et al.*, 2005]. The wetland centric view is supported by a number of model studies that appear to show that τ has changed relatively little despite the large changes in the global methane burden and sink between preindustrial and modern times [*Crutzen and Bruhl*, 1993; *Lelieveld et al.*, 1998; *Martinerie et al.*, 1995; *Shindell et al.*, 2003; *Thompson*, 1992; *Wang and Jacob*, 1998]. Measurements of methyl chloroform (MCF; CH_3CCl_3) since 1978 are used to determine modern OH concentrations. These data show that while there can be significant interannual variability in OH, the longer term trend is small [*Bousquet et al.*, 2005], despite rising methane levels. This supports the contention that OH, the main sink for CH_4, has been relatively stable in the past and implies that the concentration changes we observe are likely to be the result of source changes. However, no tracer of past changes in global OH levels before MCF measurements began in 1978 currently exists, and therefore the ultimate validity of this argument remains to be tested. This is important given that the magnitude of the interannual global methane sink due to reaction with OH [*Bousquet et al.*, 2006] is of a similar magnitude to the multidecadal variability seen in the LPIH.

3.2.2. Methane Source Variations

[27] If we assume that the methane sink has remained relatively constant then the observed multidecadal variability would be a result of variations in source strength. Methane is primarily produced by the anaerobic decomposition of organic material by archaea (see *Khalil* [2000] for a review). To obtain a source distribution for the LPIH, we combined the "Holocene base" scenario from *Harder et al.* [2007], which estimates natural methane sources (~230 Tg CH_4 yr^{-1}) with the anthropogenic source estimate (~30 Tg CH_4 yr^{-1}) from *Houweling et al.* [2000], then scaled the total source to 250 Tg CH_4 yr^{-1}, as shown in Table 1. The magnitude of variability observed in the WDC05A record is ~10–34 ppb, equivalent to 4–12 Tg CH_4 yr^{-1}, or 1.4–4.8% of the total budget (Figure 2). As mentioned previously, ice cores record a smoothed history of atmospheric methane with the degree of smoothing being dependant on the characteristics of the ice core site. The Law Dome record appears to have recorded ~10–20% greater variability than WDC05A, so our record provides a constraint on the minimum amount of variability possible. The variability in the WDC05A record is similar in magnitude to each of the individual nonwetland sources (Table 1). Since it is unlikely that the multidecadal variability comes from very large changes in the smaller budget terms, the most likely explanation is that the variability comes from emissions from wetlands which, given adequate carbonaceous substrate, are predominantly influenced by water table depth and soil temperature [e.g., *Allen et al.*, 2003; *Bloom et al.*, 2010; *Christensen et al.*, 2004; *Matthews*, 2000; *van Hulzen et al.*, 1999; *Walter et al.*, 2001a, 2001b; *Wang et al.*, 2009; *Worthy et al.*, 2000; *Zona et al.*, 2009]. Sufficient water is required to produce anoxic conditions that are a prerequisite for methanogenesis. Once anoxic conditions are present, increasing temperatures lead to higher emissions with a maximum growth temperature of 37°C–45°C [*Boone*, 2000]. Temperature and precipitation controls on methanogenesis operate on subannual timescales, so changes in these climatic variables have an immediate impact on annual emissions. The record of methane emissions is then smoothed by the atmosphere and by the firn before being trapped in polar ice sheets. Wetland emissions are thus controlled by temperature and precipitation changes and respond quickly (on subannual timescales) to changes in these variables, so we would expect the ice core methane record to be correlated with temperature and precipitation changes on multidecadal timescales.

[28] In sections 3.2.2.1 and 3.2.2.2 we examine LPIH temperature and precipitation records as well as estimates of anthropogenic emissions for relationships with the WDC05A methane record. Our approach is guided by modeling studies and satellite measurements which show that precipitation exerts a dominant control on tropical (30°S–30°N) methane emission variability through its influence on water table depth and interannual OH concentrations, whereas temperature is the dominant factor in high latitude northern hemisphere (30°N–90°N) variability [*Bekki and Law*, 1997; *Bloom et al.*, 2010; *Bousquet et al.*, 2006; *Khalil and Rasmussen*, 1983; *Walter et al.*, 2001a]. Prior to comparison, the paleoclimate records and the methane record were smoothed with a band-pass filter removing periods shorter than 20 years and longer than 500 years, removing variability both higher than the Nyquist frequency of the ice core record and lower than multicentennial frequencies due to slow changes in forcing (e.g., gradual cooling between the Medieval Warm Period and the Little Ice Age), isolating variability on multidecadal timescales. To calculate correlations and their statistical significance ($p < 0.05$, null hypothesis that $r = 0$), the smoothed paleoclimate records were then subsampled to match the ages of our methane data points ($N = 89$).

3.2.2.1. Temperature

[29] Previous studies have documented the striking correlation between the oxygen isotope record of ice ($\delta^{18}O_{ice}$, a

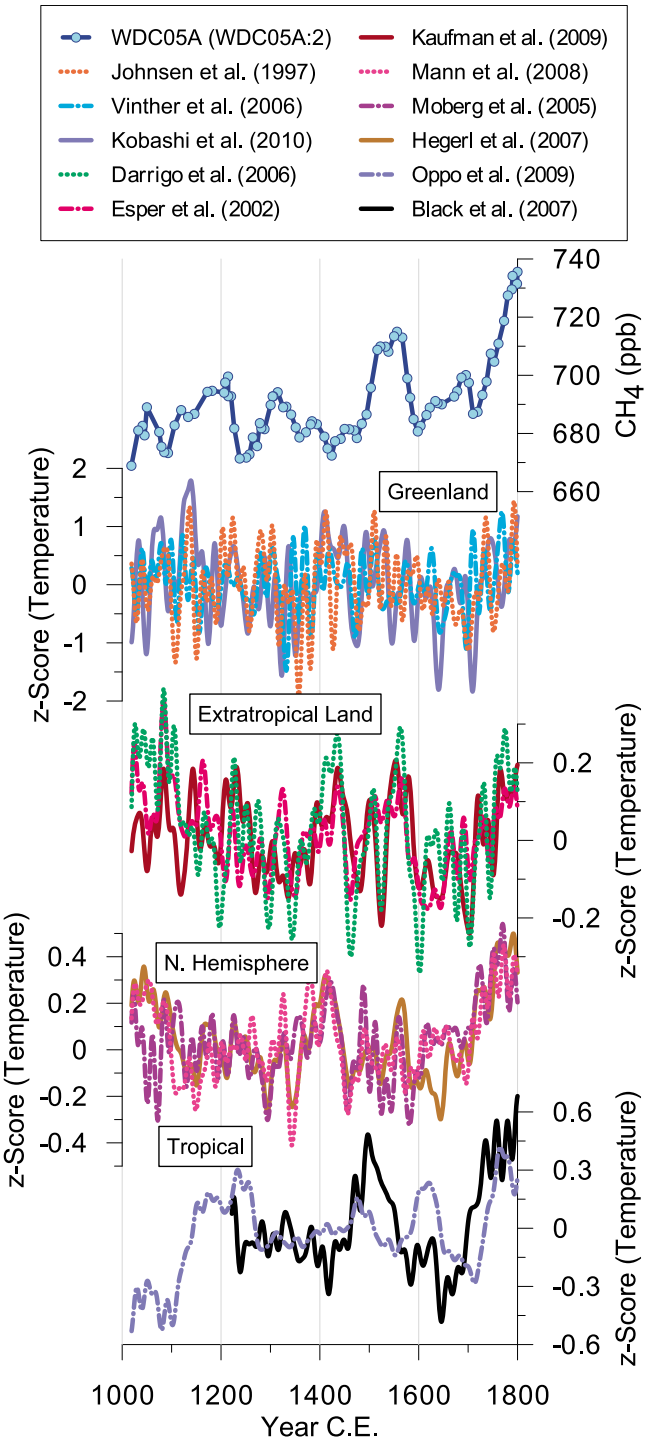

Figure 4. Comparison between WDC05A methane concentrations on the WDC05A:2 chronology and temperature reconstructions. Greenland: orange, dotted [*Johnsen et al.*, 1997]; light blue, dash-dotted [*Vinther et al.*, 2006]; dark blue, solid [*Kobashi et al.*, 2010]. Extratropical land: green, dotted [*D'Arrigo et al.*, 2006]; light red, dash-dotted [*Esper et al.*, 2002]; dark red, solid [*Kaufman et al.*, 2009]. N. Hemisphere: pink, dotted [*Mann et al.*, 2008]; purple, dash-dotted [*Moberg et al.*, 2005]; brown, solid [*Hegerl et al.*, 2007]. Tropical: blue, dash-dotted [*Oppo et al.*, 2009]; black, solid [*Black et al.*, 2007]. All records were smoothed with a band-pass filter with a period of 20–500 years.

proxy for local temperature) from Greenland ice cores and methane during the past glacial cycle [e.g., *Brook et al.*, 2000; *Chappellaz et al.*, 1993; *Huber et al.*, 2006; *Severinghaus and Brook*, 1999; *Severinghaus et al.*, 1998]. See Table 2 and Figure 4 for comparisons between methane and temperature proxies. The correlation coefficient between our methane record and the GRIP [*Johnsen et al.*, 1997] $\delta^{18}O_{ice}$ record is statistically significant, but not high ($r = 0.24$, $p = 0.03$). The correlation coefficient is even lower and not statistically significant with the NGRIP [*Vinther et al.*, 2006] $\delta^{18}O_{ice}$ record ($r = 0.06$, $p = 0.56$). A record of temperature reconstructed from $\delta^{40}Ar$ and $\delta^{15}N$ isotopes from GISP2 [*Kobashi et al.*, 2010] also does not have a statistically significant correlation with methane ($r = 0.18$, $p = 0.10$). Sliding the chronologies of these records relative to our methane record by ± 50 years does not greatly increase the correlation coefficients. We infer from this analysis that the close relationship between methane and large temperature changes during the last ice age apparently does not extend to the very small temperature variability in Greenland during the LPIH, at least to the extent that these proxies are actually recording site temperature.

[30] We have also compared our record to three northern hemispheric land temperature reconstructions [*Mann et al.*, 2008] EIV Land ($r = -0.10$, $p = 0.37$) [*Moberg et al.*, 2005] ($r = -0.13$, $p = 0.23$) [*Hegerl et al.*, 2007] ($r = 0.03$, $p = 0.81$) (Table 2 and Figure 4). The weakly negative correlation coefficients and lack of statistical significance indicates that hemispheric temperature variability during the LPIH did not directly control global methane concentrations. Hemispheric to global temperature reconstructions have been used to scale methane emissions in model reconstructions for the late Holocene using the argument that emissions are temperature sensitive and because of a lack of other constraints [*Houweling et al.*, 2008]. Our results suggest that this approach will not yield accurate results.

[31] Local- to regional-scale temperature reconstructions that are specific to methane source regions might be expected to have a greater correlation with global methane concentrations. Analysis of modern methane emissions indicates that Northern Hemisphere extratropical wetlands are more sensitive to temperature than tropical wetlands [*Bloom et al.*, 2010]. We examined two extratropical Northern Hemisphere temperature reconstructions [*D'Arrigo et al.*, 2006] ($r = 0.04$, $p = 0.73$) and [*Esper et al.*, 2002] ($r = 0.16$, $p = 0.13$) that utilize similar data sets and found that they both have low correlation coefficients with methane that lack statistical significance. A multiproxy Arctic temperature reconstruction [*Kaufman et al.*, 2009] ($r = 0.24$, $p = 0.03$) has a low but statistically significant correlation with methane which increases to $r = 0.34$ if the record is interpolated annually and shifted by −30 years, within the uncertainty in their chronology (~2–10%).

[32] We also examine correlation coefficients with tropical sea surface temperature records from the Indo Pacific Warm Pool (IPWP) [*Oppo et al.*, 2009] ($r = 0.26$, $p = 0.01$) and Cariaco Basin [*Black et al.*, 2007] ($r = 0.35$, $p < 0.01$) and find statistically significant correlation coefficients that are slightly higher than with other temperature reconstructions. The record from the Cariaco basin has a high correlation ($r = 0.77$) when the record is interpolated annually and shifted forward in time by 52 years. The magnitude of this

Table 2. Linear Correlation Coefficients (r) Between Temperature Reconstructions, Precipitation Proxy Records, and the WDC05A Methane Record[a]

Source	Region	r	p
	Temperature Proxy Records and Reconstructions		
Johnsen et al. [1997]	Greenland (GRIP)	0.24	0.03
Vinther et al. [2006]	Greenland (NGRIP)	0.06	0.56
Kobashi et al. [2010]	Greenland (GISP2)	0.18	0.10
D'Arrigo et al. [2006]	Extratropical N.H. 40°N–90°N	0.04	0.73
Esper et al. [2002]	Extratropical N.H. 30°N–90°N	0.16	0.13
Kaufman et al. [2009]	Extratropical N.H. 60°N–90°N	0.24	0.03
Mann et al. [2008] EIV Land	Northern Hemisphere	−0.10	0.37
Moberg et al. [2005]	Northern Hemisphere	−0.13	0.23
Hegerl et al. [2007]	Northern Hemisphere	0.03	0.81
Oppo et al. [2009]	Tropical SST (Indo-Pacific Warm Pool)	0.26	0.01
Black et al. [2007]	Tropical SST (Cariaco Basin)	0.35	<0.01
Trouet et al. [2009]	North Atlantic Oscillation	0.03	0.76
MacDonald and Case [2005]	Pacific Decadal Oscillation	0.35	<0.01
	Precipitation Proxy Records		
Hu et al. [2008]	China Speleothem δ^{18}O (Heshang)	0.24	0.02
Wang et al. [2005]	China Speleothem δ^{18}O (Dongge)	0.02	0.88
Zhang et al. [2008]	China Speleothem δ^{18}O (Wanxiang)	0.28	0.01
Reuter et al. [2009]	Peru Speleothem δ^{18}O (Cascayunga)	−0.19	0.09

[a]All records were smoothed with a band-pass filter removing periods shorter than 20 years and longer than 500 years and then subsampled to match the ages of the WDC05A methane data (N = 89). Correlation coefficients are statistically significant when $p < 0.05$ (null hypothesis is that $r = 0$).

shift is near the chronological uncertainty for this record, which was determined by correlation to a nearby sediment core that utilizes AMS ^{14}C dates with uncertainties of ± 50–60 years [*Black et al.*, 1999]. This possible correlation on multidecadal timescales is compelling because Cariaco SSTs were highly correlated with methane and Greenland δ^{18}O records during the last glacial termination [*Lea et al.*, 2003]. Since temperature variations of the magnitude seen in this record would not be expected to have a direct impact on tropical methane emissions, we suggest that temperatures in these areas are likely linked to larger-scale climatic processes which control precipitation and more likely impacted emissions.

[33] Recently, *Mann et al.* [2009] used a diverse multiproxy network to reconstruct a global surface temperature field using a Regularized Expectation-Maximization Climate Field Reconstruction (RegEM CFR) approach. In Figure 5a we show the correlation coefficient field between band-pass-filtered and subsampled surface temperature and methane during the LPIH. Hatching indicates statistically significant correlation ($p < 0.05$, null hypothesis is that $r = 0$) in that grid box. The highest, statistically significant correlation coefficients exist in the eastern tropical, southern, and northern Pacific, and extratropical Eurasia. Negative correlation coefficients exist over the north Atlantic. The proxy network used in this reconstruction has very few oceanic records so oceanic temperatures are dependent on the covariance relationships established with the CFR approach which assumes temporal stationarity between proxy indicators and large-scale climate patterns [*Mann et al.*, 2008]. Since the ocean is a negligible source of methane, the correlations with oceanic SSTs indicate possible relationships with climate variability on multidecadal timescales associated with SSTs in those areas. The positive correlations over extratropical Eurasia are consistent with the hypothesis that temperature variability in this region is a controlling factor on emissions and impacts multidecadal variability of global methane concentrations. This same relationship has been

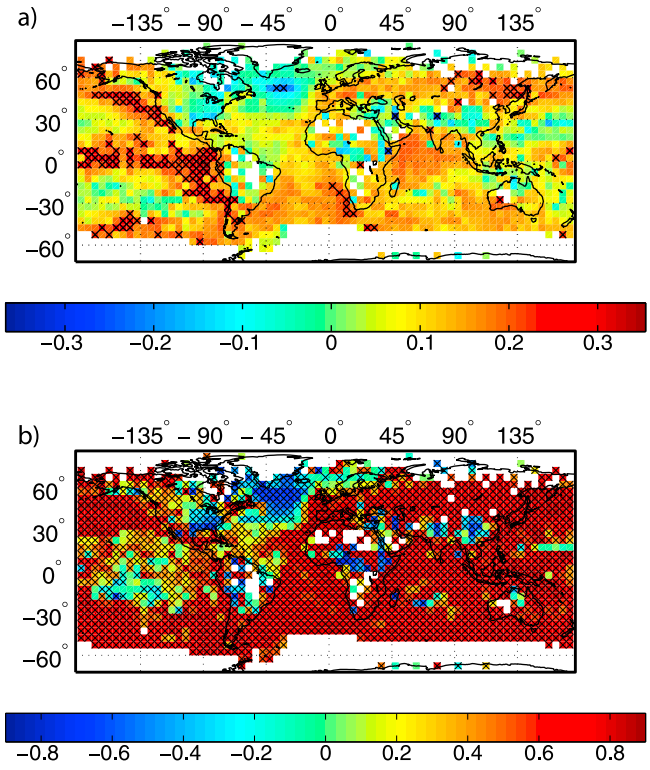

Figure 5. Correlation (r) between WDC05A methane concentrations on the WDC05A:2 chronology and reconstructed 5° × 5° gridded surface temperature [*Mann et al.*, 2009] for (a) the LPIH (1000–1800 C.E.) and (b) 1400–1600 C.E. Prior to comparison, the surface temperatures were smoothed with a band-pass filter with a period of 20 to 500 years. Hatching indicates statistically significant correlation ($p < 0.05$, null hypothesis is that $r = 0$) in that grid box.

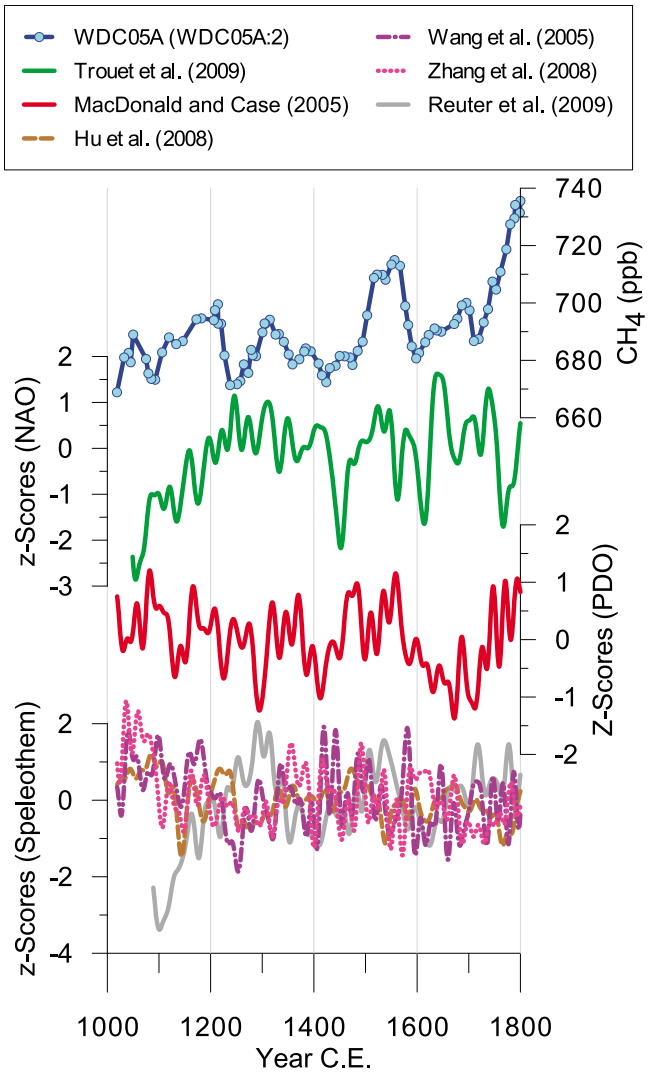

Figure 6. Comparison between WDC05A methane concentrations on the WDC05A:2 chronology and paleoproxies for precipitation. Smoothing applied to all records is discussed in the text. From top to bottom are WDC05A CH_4 (this study); NAO index [*Trouet et al.*, 2009]; PDO index [*MacDonald and Case*, 2005]; Speleothem records from the East Asian Monsoon: Heshang (brown, dashed) [*Hu et al.*, 2008], Dongge (purple, dash-dotted) [*Wang et al.*, 2005], Wanxiang (pink, dotted) [*Zhang et al.*, 2008]. Speleothem record from Peru: Cascayunga (gray) [*Reuter et al.*, 2009]. All records were smoothed with a band-pass filter with a period of 20–500 years.

observed on interannual and shorter timescales by satellite measurements in recent years [*Bloom et al.*, 2010].

[34] The Pacific Decadal Oscillation (PDO) is a leading mode of variability in the North Pacific that exhibits multidecadal variability affecting regional SSTs and precipitation patterns [*Mantua and Hare*, 2002; *Mantua et al.*, 1997]. A PDO reconstruction covering the LPIH [*MacDonald and Case*, 2005] ($r = 0.35$, $p = < 0.01$) has a moderate, statistically significant correlation with methane (Table 2 and Figure 6). The positive correlations with tropical Pacific SSTs and the PDO index are puzzling since on interannual timescales La Niña conditions (when SSTs are anomalously cold in this region) are associated with greater precipitation over tropical land areas and greater tropical methane emissions [*Dlugokencky et al.*, 2009; *Gu et al.*, 2007]. We also examined a proxy for the North Atlantic Oscillation (NAO) [*Trouet et al.*, 2009] ($r = 0.03$, $p = 0.76$); however, this proxy has no correlation with methane on multidecadal timescales.

[35] The positive correlations we observe between temperature reconstructions in some regions and the methane record appear to be driven in large part by temperature variations in the latter part of the record, particularly between 1400 and 1600 C.E. The largest feature in our methane record for the LPIH is a large increase from 1470 to 1520 and a subsequent decrease from 1560 to 1600 C.E. A similar feature is seen in many temperature reconstructions; however, the temperature decline is seen most prominently in records from higher latitudes: Sweden [*Grudd et al.*, 2002]; north (55°–70°N) and eastern hemisphere regions [*Cook et al.*, 2004]; northern Siberia [*Briffa et al.*, 2001]; Yukon, Central Northwest Territories, Jaemtland, Tornetraesk, and Mongolia [*D'Arrigo et al.*, 2006]; modeled Arctic temperatures calibrated to Arctic temperature proxies [*Crespin et al.*, 2009]. The fall in methane is also coincident with the start of the "classical" climatological Little Ice Age (LIA) [*Matthews and Briffa*, 2005]. Using the temperature field reconstruction discussed above [*Mann et al.*, 2009], we used the annually interpolated records to calculate correlation coefficients in 200 year moving windows and found the highest correlation during the time period 1400–1600 C.E. (Figure 5b). During this time period the land region with the greatest spatially consistent statistically significant positive correlations is extratropical Eurasia. These observations suggest that temperature perturbations in this time period, particularly in the high latitude northern hemisphere, may have impacted global methane concentrations as has been noted previously by other workers [*Etheridge et al.*, 1998; *MacFarling Meure et al.*, 2006].

3.2.2.2. Precipitation

[36] The largest areas of methane emissions from natural wetlands are the monsoon regions of East Asia, India, and South America [*Bergamaschi et al.*, 2009]. High temporal resolution records of rainfall variability in specific areas of monsoon regions have been inferred from the oxygen isotopic composition ($\delta^{18}O$) of speleothems (cave deposits). While the correlation between speleothems from monsoon regions to Greenland temperature [e.g., *Wang et al.*, 2006; *Wang et al.*, 2001] and Greenland temperature to methane [e.g., *Brook et al.*, 2000; *Chappellaz et al.*, 1993] have been widely reported for the last ice age, these relationships have not been explored for the late Holocene.

[37] Speleothem $\delta^{18}O$ records that cover the LPIH with enough temporal resolution to observe multidecadal variability have been recovered from the East Asian monsoon region and Peru. Of the East Asian speleothem records, the Dongge [*Wang et al.*, 2005] and Heshang [*Hu et al.*, 2008] chronologies have uncertainties of ± 50 years which reduces the confidence in the timing of multidecadal variability. The Wanxiang [*Zhang et al.*, 2008] chronology is much better (< ± 5 years) and is highly correlated on decadal timescales with another speleothem from the Dandak cave in east central India [*Berkelhammer et al.*, 2010] which supports

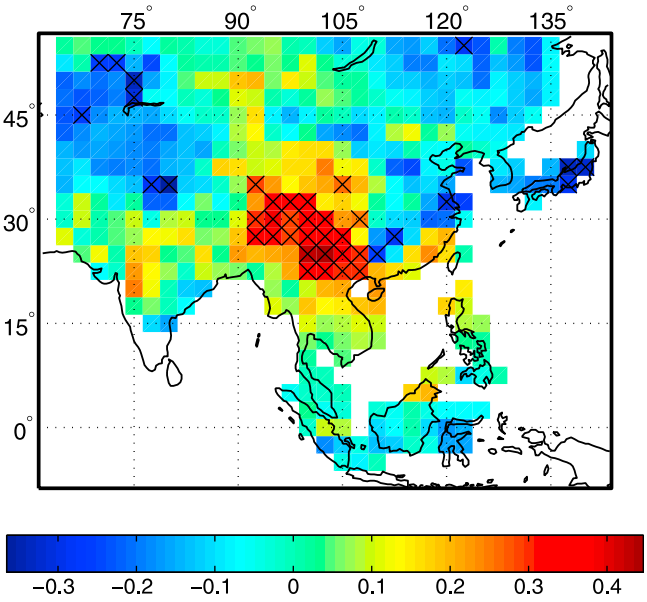

Figure 7. Correlation (r) between WDC05A methane concentrations on the WDC05A:2 chronology and 2.5° × 2.5° gridded Palmer Drought Severity Index (PDSI) [*Cook et al.*, 2010] between 1300 and 1800 C.E. Prior to comparison, the PDSI indices were smoothed with a band-pass filter with a period of 20 to 500 years. Hatching indicates statistically significant correlation ($p < 0.05$, null hypothesis is that $r = 0$) in that grid box.

the interpretation that these records represent regional precipitation. On their stated chronologies, the Heshang ($r = 0.24$, $p = 0.02$) and Wanxiang ($r = 0.28$, $p = 0.01$) speleothem $\delta^{18}O$ records have statistically significant correlation with methane, but the Dongge ($r = 0.02$, $p = 0.88$) record does not (Table 2 and Figure 6). The speleothem $\delta^{18}O$ record from the Cascayunga cave in Peru is inversely correlated with tropical SSTs in the Cariaco basin on multidecadal timescales [*Reuter et al.*, 2009] and other South American speleothems have shown this same relationship on millennial timescales [*Cruz et al.*, 2005; *Lea et al.*, 2003]. Correlation between methane and the Cascayunga speleothem is negative and is not statistically significant on its stated chronology ($r = -0.19$, $p = 0.09$). The correlation increases to $r = -0.35$ when the annually interpolated chronology is shifted forward in time by 19 years, although this shift is larger than the uncertainty of their chronology (±4–9 years) [*Reuter et al.*, 2009]. This possible correlation on multidecadal timescales is intriguing because a negative correlation has been noted between South American speleothems and methane on millennial timescales [*Cruz et al.*, 2005].

[38] A recent spatial reconstruction of the Asian monsoon region Palmer Drought Severity Index (PDSI) using tree rings [*Cook et al.*, 2010] extends back to 1300 C.E. and offers a significant advancement in that the records are annually resolved and have a broad distribution over a large wetland region. Spatial correlation coefficients and analytical uncertainty from this reconstruction were constructed in the same manner as the correlation with the temperature field reconstruction and cover 1300–1800 C.E. (Figure 7). Positive PDSI values indicate wetter conditions and the highest positive correlation coefficients are centered on the eastern Tibetan Plateau. This area is the source of many major Asian rivers (Yangtze, Mekong, Yellow, Pearl, and Salween rivers) which feed much of the Asian monsoon region. Modern satellite observations show that this area is also a major source of methane emissions which are positively correlated with groundwater depth and temperature on interannual and shorter timescales [*Bergamaschi et al.*, 2009; *Bloom et al.*, 2010]. Our results suggest that the relationship between methane and drought in this area holds for multidecadal timescales and may have been an important factor contributing to global methane variability during the LPIH.

3.2.2.3. Anthropogenic Methane Sources

[39] The dramatic increase in atmospheric methane concentrations at the start of the industrial revolution in the mid-18th century is a result of increasing anthropogenic emissions. Before this time the contribution of anthropogenic emissions are not well constrained [*Ferretti et al.*, 2005; *Houweling et al.*, 2008; *Mischler et al.*, 2009]. A range of published LPIH anthropogenic methane emissions are shown in Table 3. These estimates are generally constructed by scaling modern anthropogenic emissions down with population and then making educated guesses about how anthropogenic activities (land use, farming practices, etc.) would have altered per capita emissions. The process involves many difficult to verify assumptions and we thus caution that the exact value of the following semiquantitative calculations is less important than the approximate magnitudes.

[40] The "early anthropogenic" hypothesis argues that human activity began altering atmospheric methane concentrations as early as 5000 years ago with the biggest contribution coming from agricultural activities, particularly rice farming in China [see *Ruddiman*, 2003, 2007, and references therein]. The hypothesis presumes that early rice farming techniques were inefficient resulting in disproportionately large methane emissions per capita relative to modern times. Following this line of reasoning, any large reduction in human population or agricultural production during the LPIH caused by plagues or wars, especially in areas of rice cultivation, should have reduced methane emissions on the timescales of those events. Here we use the historic record to explore the possibility that reductions in human populations, agricultural production, or land use patterns were large enough to have a demonstrative impact on global methane concentrations.

[41] The two biggest wars in Asia during the LPIH were the Mongol invasion beginning in 1211 C.E. lasting for about three decades, and the overthrow of Ming dynasty and the establishment of the Qing dynasty in the mid-17th century. These events were associated with large losses of population estimated at 35 million (~30% or ~15% of the total Chinese or Asian population, respectively) during the Mongol invasion and 25 million (~15% or ~7% of the total Chinese or Asian population, respectively) during the transition between the Ming and Qing dynasties [*McEvedy and Jones*, 1978; *Pongratz et al.*, 2008]. *Zhang et al.* [2007] examined agricultural production associated with wars in China from 1500 to 1800 C.E. and concluded that the war and loss of human life associated with the transition between

Table 3. Estimates of Anthropogenic Emissions at ~1500 C.E.[a]

	Houweling et al. [2000] and *Houweling et al.* [2008]	*Ruddiman* [2007]	*Ferretti et al.* [2005]	*Subak* [1994]	*Mischler et al.* [2009]
Rice agriculture	10	~28 (23–32)	-	15	15
Biomass burning	10	20	~20	30 (26 = biomass; 4 = wood fuel)	38
Domestic Ruminants	5	7	-	10	-
Waste	5	4	-	-	-
Climate feedbacks	-	~10 (6–15)	-	-	-
Total	30	~69 (60–78)	~20	55	53
Percent of total budget	12	~28	~8	22	21

[a]In Tg CH_4 yr^{-1}. Dashes indicate that the study did not estimate that source. Total budget is assumed to be 250 Tg CH_4 yr^{-1}.

the Ming and Qing dynasties resulted in a sharp decrease in agricultural production. The invasion of the Mongol armies would have resulted in a similar or larger decrease in agricultural production due to the greater percentage of the population that was killed.

[42] Assuming that essentially all preindustrial rice production occurred in Asia and given that~70% of the total world population lived in Asia [*McEvedy and Jones*, 1978], we can add 100% of the rice emissions and 70% of all other anthropogenic emissions (Table 3) to estimate Asian anthropogenic emissions. Here we will focus on the high and low estimates of anthropogenic emissions that are commonly cited in the literature. This leads to estimates of Asian anthropogenic emissions of ~24 Tg CH_4 yr^{-1} based on the work by *Houweling et al.* [2000] and ~56 Tg CH_4 yr^{-1} based on the work by *Ruddiman* [2007]. Assuming a linear scaling between Asian population change and anthropogenic methane emissions, the invasion of the Mongol armies during ~1211–1241 C.E. would have resulted in a reduction of ~3.3–7.9 Tg CH_4 yr^{-1} or ~10–23 ppb for *Houweling et al.*'s [2000] and *Ruddiman*'s [2007] estimates, respectively. The WDC05A record shows that methane decreased by ~25–30 ppb from 1218 to 1235 C.E. Using the same argument, the transition from the Ming to Qing dynasties (1618–1662 C.E.) would have led to a reduction of ~1.6–3.7 Tg CH_4 yr^{-1} or ~5–11 ppb for *Houweling et al.*'s [2000] and *Ruddiman*'s [2007] estimates, respectively. The WDC05A record has a small gap during this time period, but there is a decrease of ~13 ppb observed in the Law Dome record. Preliminary measurements from the main borehole (WDC06A) have a decrease similar to Law Dome (not shown) in this time interval. Therefore the timing and magnitude of putative reductions in anthropogenic rice emissions resulting from war is within the chronology uncertainty of our record and represents a possible cause for these reductions in methane.

[43] There is further anecdotal evidence that the invasion of the Mongol empire could have influenced methane emissions. After razing villages and cities, the Mongol army laboriously dismantled the irrigation systems and used their horses to churn up the soil [*Weatherford*, 2004]. This prevented people from immediately resettling after the Mongol army left and also allowed the land to revert to grasslands which have significantly lower methane emissions than irrigated farmland. Following the invasion, the governing Mongols encouraged scientific innovations which led in 1261 C.E. to the establishment of the Office for the Stimulation of Agriculture which sought to increase the agricultural output of farmlands by the diversification of crops and improvement of farming practices [*Weatherford*, 2004]. At this same time, global methane concentrations began to increase. These land use changes would have changed the areal extent of methane emissions, and we speculate that it could have contributed to the rapid changes in global methane concentrations during this time period.

[44] In the mid-14th century, plague broke out and spread rapidly across Asia and Europe along the extensive Mongol trade network. Population losses in Asia and Europe were estimated to be in excess of 60 million and 20 million, respectively [*McEvedy and Jones*, 1978; *Weatherford*, 2004]. Use of the linear scaling argument above leads to a reduction of Asian anthropogenic emissions of ~6–14.3 Tg CH_4 yr^{-1} and European anthropogenic emissions of ~1.5–3.3 Tg CH_4 yr^{-1} for *Houweling et al.*'s [2000] and *Ruddiman*'s [2007] estimates, respectively. Thus the total reduction by linear scaling caused by plague would have been ~7.5–17.6 Tg CH_4 yr^{-1} or ~21–50 ppb. The WDC05A record shows that methane decreases by ~16 ppb from 1314 to 1359 C.E. A possible explanation for the smaller than estimated reduction in methane is that plague would not have caused the land use changes that occurred during wars. This suggests that the land use changes could have had a greater impact than population changes and might be an explanation for why the reduction in methane during the Mongol invasion is slightly greater than that estimated with a linear scaling to population.

[45] Changes in the $\delta^{13}CH_4$ record can help identify methane sources which have divergent isotopic signatures. The $\delta^{13}CH_4$ record over the LPIH shows a large, gradual decrease from 1400 to 1700 C.E.; however, a large portion of the decrease occurs during 1560–1600 C.E. [*Ferretti et al.*, 2005; *Mischler et al.*, 2009]. This is coincident with the largest decrease in methane concentrations during the LPIH, ~32 ppb in the WDC05A record. *Ferretti et al.* [2005] proposed that the reduction in $\delta^{13}CH_4$ was caused by the decrease of biomass burning (an isotopically heavy source) in the Americas after the arrival of European settlers introduced disease to Native American populations causing a widespread pandemic [*Cook*, 1998; *Ruddiman*, 2007]. This hypothesis is consistent with a marked decrease in charcoal accumulation in global sedimentary records [*Marlon et al.*, 2008]. Estimates of LPIH biomass burning emissions range from 10 to 38 Tg CH_4 yr^{-1} which corresponds to 28–108 ppb (Table 3). While these estimates include some anthropogenic biomass burning that is outside of North America, *Ferretti et al.* [2005] argue that Native American activities provided the greatest contribution to this source. Thus a reduction in biomass burning methane

emissions during this time period is consistent with three independent lines of evidence: the decrease in methane concentrations, decreasing isotopic $\delta^{13}CH_4$ values, and widespread pandemics in the Americas associated with European invasion.

[46] While anthropogenic activities may have had a discernable impact on multidecadal variations in methane concentrations, many uncertainties remain. Past population estimates are highly uncertain, particularly for the precolonial Americas and Asia. Additional work on quantifying the range of emissions from modern and preindustrial rice agriculture techniques as well as the extent of rice agriculture in the LPIH is needed. Longer high-precision methane records can place the LPIH variations in a longer term context. A coupling of methane emissions with anthropogenic activities could be an explanation for the generally low correlations with temperature and precipitation reconstructions over the LPIH discussed earlier.

4. Conclusion

[47] We have presented a new high-resolution, high-precision record of atmospheric methane covering 1000–1800 C.E. from the West Antarctic Ice Sheet Divide ice core (WDC05A). The high correlation between the WDC05A and the Law Dome methane record [*Etheridge et al.*, 1998; *MacFarling Meure et al.*, 2006] confirms the variability observed in both records. We are able to uniquely identify small-scale variability demonstrating that high-resolution methane records can be used to establish chronostratigraphic tie points for ice core gas chronologies on short timescales.

[48] We find that reconstructions of regional to hemispheric temperature are not highly correlated with methane concentrations. Correlation coefficients with a spatially resolved temperature reconstruction are highest in northern Eurasia, consistent with modern satellite observations on interannual timescales. The highest correlation coefficients with the spatial temperature reconstruction as well as many individual extratropical northern hemisphere temperature reconstructions are observed from 1400 to 1600 C.E. during the onset of the Little Ice Age. This suggests that temperature variations during this time period impacted methane variations. The correlation between proxies for East Asian monsoon strength and methane are similarly low on multidecadal timescales, although uncertainty in the age scales prevents a definitive analysis in some cases. A spatial reconstruction of the Asian monsoon region Palmer Drought Severity Index has the greatest correlation with methane at the headwaters of major East Asian rivers, consistent with modern satellite observations. Moderate to high correlations exist with a Peruvian speleothem and tropical SSTs in the Cariaco basin if these records are shifted by the maximum amount allowed by the uncertainty in their chronologies. These possible correlations on multidecadal timescales are compelling because these relationships have been documented on millennial timescales and suggest that they could be a robust feature of the climate system. Possible explanations for the lack of high correlations with temperature and precipitation proxies are that the individual records comprising these reconstructions may not be reflecting conditions in methane source regions or that the variations were not large enough to significantly perturb methane emissions. Anthropogenic activities could have affected methane emissions based on the synchronous timing between large population losses in Asia and the Americas and decreases in methane concentrations. Our work reinforces the need for additional absolutely dated paleoclimate proxies [*Jones et al.*, 2009], particularly from methane source regions.

[49] Future work will involve extending the high-resolution WAIS Divide methane record beyond 1000 C.E. using the main borehole WDC06A. Extension of the record will characterize the frequency of methane variability and changes in multidecadal variability that may be caused by variations in climate or anthropogenic activities. Understanding high-precision methane variability is critical for placing the recent record of atmospheric and satellite measurements in a longer term context, increasing our understanding of the range of variability in the global methane budget, and for prediction of future changes in that budget. Very high resolution records of methane from Greenland are needed to characterize multidecadal and centennial variability in the Inter Polar Gradient which will provide another constraint on the global methane budget.

[50] **Acknowledgments.** This work was supported by NSF OPP grants 0538578, 0520523, and 0538538 and by NASA/Oregon Space Grant Consortium grant NNG05GJ85H. Glaciochemical dating of the WDC05A and WDC06A ice cores was supported by NSF OPP grants 0538427 and 0739780 to the Desert Research Institute. Thanks go to James Lee, who assisted with the methane measurements; Nelia Dunbar, Mark Battle, Jeff Severinghaus, and Eric Steig, who contributed preliminary results from their work; and two anonymous reviewers, who provided insightful feedback that improved this manuscript. The authors appreciate the support of the WAIS Divide Science Coordination Office at the Desert Research Institute of Reno Nevada for the collection and distribution of the WAIS Divide ice core and related tasks (Kendrick Taylor, NSF grants 0440817 and 0230396). The National Science Foundation Office of Polar Programs also funds the Ice Drilling Program Office and Ice Drilling Design and Operations group for coring activities; Raytheon Polar Services for logistics support in Antarctica; and the 109th New York Air National Guard for airlift in Antarctica. The National Ice Core Laboratory, which curated the core and preformed core processing, is jointly funded by the National Science Foundation and the U.S. Geological Survey. Data and description can be downloaded from the NOAA National Climate Data Center http://www.ncdc.noaa.gov/paleo/paleo.html.

References

Allen, L. H., S. L. Albrecht, W. Colon-Guasp, S. A. Covell, J. T. Baker, D. Y. Pan, and K. J. Boote (2003), Methane emissions of rice increased by elevated carbon dioxide and temperature, *J. Environ. Qual.*, *32*(6), 1978–1991, doi:10.2134/jeq2003.1978.

Banta, J. R., J. R. McConnell, M. M. Frey, R. C. Bales, and K. Taylor (2008), Spatial and temporal variability in snow accumulation at the West Antarctic Ice Sheet Divide over recent centuries, *J. Geophys. Res.*, *113*, D23102, doi:10.1029/2008JD010235.

Battle, M., et al. (1996), Atmospheric gas concentrations over the past century measured in air from firn at the South Pole, *Nature*, *383*(6597), 231–235, doi:10.1038/383231a0.

Bekki, S., and K. S. Law (1997), Sensitivity of the atmospheric CH_4 growth rate to global temperature changes observed from 1980 to 1992, *Tellus, Ser. B*, *49*(4), 409–416, doi:10.1034/j.1600-0889.49.issue4.6.x.

Bergamaschi, P., et al. (2009), Inverse modeling of global and regional CH_4 emissions using SCIAMACHY satellite retrievals, *J. Geophys. Res.*, *114*, D22301, doi:10.1029/2009JD012287.

Berkelhammer, M., A. Sinha, M. Mudelsee, H. Cheng, R. L. Edwards, and K. Cannariato (2010), Persistent multidecadal power of the Indian summer monsoon, *Earth Planet. Sci. Lett.*, *290*(1–2), 166–172, doi:10.1016/j.epsl.2009.12.017.

Black, D. E., L. C. Peterson, J. T. Overpeck, A. Kaplan, M. N. Evans, and M. Kashgarian (1999), Eight centuries of North Atlantic Ocean

atmosphere variability, *Science*, *286*(5445), 1709–1713, doi:10.1126/science.286.5445.1709.

Black, D. E., M. A. Abahazi, R. C. Thunell, A. Kaplan, E. J. Tappa, and L. C. Peterson (2007), An 8-century tropical Atlantic SST record from the Cariaco Basin: Baseline variability, twentieth-century warming, and Atlantic hurricane frequency, *Paleoceanography*, *22*, PA4204, doi:10.1029/2007PA001427.

Bloom, A. A., P. I. Palmer, A. Fraser, D. S. Reay, and C. Frankenberg (2010), Large-scale controls of methanogenesis inferred from methane and gravity spaceborne data, *Science*, *327*(5963), 322–325, doi:10.1126/science.1175176.

Blunier, T., and E. J. Brook (2001), Timing of millennial-scale climate change in Antarctica and Greenland during the last glacial period, *Science*, *291*(5501), 109–112, doi:10.1126/science.291.5501.109.

Boone, C. D. (2000), Biological formation and consumption of methane, in *Atmospheric Methane: Its Role in the Global Environment*, edited by M. A. K. Khalil, pp. 42–62, Springer, New York.

Bousquet, P., D. A. Hauglustaine, P. Peylin, C. Carouge, and P. Ciais (2005), Two decades of OH variability as inferred by an inversion of atmospheric transport and chemistry of methyl chloroform, *Atmos. Chem. Phys.*, *5*, 2635–2656, doi:10.5194/acp-5-2635-2005.

Bousquet, P., et al. (2006), Contribution of anthropogenic and natural sources to atmospheric methane variability, *Nature*, *443*(7110), 439–443, doi:10.1038/nature05132.

Briffa, K. R., T. J. Osborn, F. H. Schweingruber, I. C. Harris, P. D. Jones, S. G. Shiyatov, and E. A. Vaganov (2001), Low-frequency temperature variations from a northern tree ring density network, *J. Geophys. Res.*, *106*, 2929–2941, doi:10.1029/2000JD900617.

Brook, E. J., S. Harder, J. Severinghaus, E. J. Steig, and C. M. Sucher (2000), On the origin and timing of rapid changes in atmospheric methane during the last glacial period, *Global Biogeochem. Cycles*, *14*(2), 559–572, doi:10.1029/1999GB001182.

Brook, E. J., J. W. C. White, A. S. M. Schilla, M. L. Bender, B. Barnett, J. P. Severinghaus, K. C. Taylor, R. B. Alley, and E. J. Steig (2005), Timing of millennial-scale climate change at Siple Dome, West Antarctica, during the last glacial period, *Quat. Sci. Rev.*, *24*(12–13), 1333–1343, doi:10.1016/j.quascirev.2005.02.002.

Chappellaz, J., T. Blunier, D. Raynaud, J. M. Barnola, J. Schwander, and B. Stauffer (1993), Synchronous changes in atmospheric CH_4 and Greenland climate between 40 and 8 kyr BP, *Nature*, *366*(6454), 443–445, doi:10.1038/366443a0.

Christensen, T. R., T. R. Johansson, H. J. Akerman, M. Mastepanov, N. Malmer, T. Friborg, P. Crill, and B. H. Svensson (2004), Thawing sub-arctic permafrost: Effects on vegetation and methane emissions, *Geophys. Res. Lett.*, *31*, L04501, doi:10.1029/2003GL018680.

Cook, E. R., J. Esper, and R. D. D'Arrigo (2004), Extra-tropical Northern Hemisphere land temperature variability over the past 1000 years, *Quat. Sci. Rev.*, *23*(20–22), 2063–2074, doi:10.1016/j.quascirev.2004.08.013.

Cook, E. R., K. J. Anchukaitis, B. M. Buckley, R. D. D'Arrigo, G. C. Jacoby, and W. E. Wright (2010), Asian monsoon failure and megadrought during the last millennium, *Science*, *328*(5977), 486–489, doi:10.1126/science.1185188.

Cook, N. D. (1998), *Born to Die: Disease and New World Conquest, 1492–1650*, 248 pp., Cambridge Univ. Press, Cambridge, U. K.

Craig, H., Y. Horibe, and T. Sowers (1988), Gravitational separation of gases and isotopes in polar ice caps, *Science*, *242*(4886), 1675–1678, doi:10.1126/science.242.4886.1675.

Crespin, E., H. Goosse, T. Fichefet, and M. E. Mann (2009), The 15th century Arctic warming in coupled model simulations with data assimilation, *Clim. Past.*, *5*(3), 389–401, doi:10.5194/cp-5-389-2009.

Crutzen, P. J., and C. Bruhl (1993), A model study of atmospheric temperatures and the concentrations of ozone, hydroxyl, and some other photochemically active gases during the glacial, the pre-industrial Holocene and the present, *Geophys. Res. Lett.*, *20*(11), 1047–1050, doi:10.1029/93GL01423.

Cruz, F. W., S. J. Burns, I. Karmann, W. D. Sharp, M. Vuille, A. O. Cardoso, J. A. Ferrari, P. L. S. Dias, and O. Viana (2005), Insolation-driven changes in atmospheric circulation over the past 116,000 years in subtropical Brazil, *Nature*, *434*(7029), 63–66, doi:10.1038/nature03365.

Cunnold, D. M., et al. (2002), In situ measurements of atmospheric methane at GAGE/AGAGE sites during 1985–2000 and resulting source inferences, *J. Geophys. Res.*, *107*(D14), 4225, doi:10.1029/2001JD001226.

D'Arrigo, R., R. Wilson, and G. Jacoby (2006), On the long-term context for late twentieth century warming, *J. Geophys. Res.*, *111*, D03103, doi:10.1029/2005JD006352.

Delmotte, M., J. Chappellaz, E. Brook, P. Yiou, J. M. Barnola, C. Goujon, D. Raynaud, and V. I. Lipenkov (2004), Atmospheric methane during the last four glacial-interglacial cycles: Rapid changes and their link with Antarctic temperature, *J. Geophys. Res.*, *109*, D12104, doi:10.1029/2003JD004417.

Dentener, F., W. Peters, M. Krol, M. van Weele, P. Bergamaschi, and J. Lelieveld (2003), Interannual variability and trend of CH_4 lifetime as a measure for OH changes in the 1979–1993 time period, *J. Geophys. Res.*, *108*(D15), 4442, doi:10.1029/2002JD002916.

Dlugokencky, E. J., L. P. Steele, P. M. Lang, and K. A. Masarie (1994), The growth rate and distribution of atmospheric methane, *J. Geophys. Res.*, *99*(D8), 17,021–17,043, doi:10.1029/94JD01245.

Dlugokencky, E. J., R. C. Myers, P. M. Lang, K. A. Masarie, A. M. Crotwell, K. W. Thoning, B. D. Hall, J. W. Elkins, and L. P. Steele (2005), Conversion of NOAA atmospheric dry air CH_4 mole fractions to a gravimetrically prepared standard scale, *J. Geophys. Res.*, *110*, D18306, doi:10.1029/2005JD006035.

Dlugokencky, E. J., et al. (2009), Observational constraints on recent increases in the atmospheric CH_4 burden, *Geophys. Res. Lett.*, *36*, L18803, doi:10.1029/2009GL039780.

Dunbar, N. W., G. A. Zielinski, and D. T. Voisins (2003), Tephra layers in the Siple Dome and Taylor Dome ice cores, Antarctica: Sources and correlations, *J. Geophys. Res.*, *108*(B8), 2374, doi:10.1029/2002JB002056.

Dunbar, N. W., W. C. McIntosh, A. V. Kurbatov, and T. I. Wilch (2007), Integrated tephrochronology of the West Antarctic region: Implications for a potential tephra record in the West Antarctic Ice Sheet (WAIS) Divide Ice Core, paper presented at WAIS Divide Science Meeting, WAIS Divide Ice Core Proj., Tahoe, N. M.

EPICA Community Members (2006), One-to-one coupling of glacial climate variability in Greenland and Antarctica, *Nature*, *444*(7116), 195–198, doi:10.1038/nature05301.

Esper, J., E. R. Cook, and F. H. Schweingruber (2002), Low-frequency signals in long tree-ring chronologies for reconstructing past temperature variability, *Science*, *295*(5563), 2250–2253, doi:10.1126/science.1066208.

Etheridge, D. M., L. P. Steele, R. J. Francey, and R. L. Langenfelds (1998), Atmospheric methane between 1000 A.D. and present: Evidence of anthropogenic emissions and climatic variability, *J. Geophys. Res.*, *103*(D13), 15,979–15,993, doi:10.1029/98JD00923.

Ferretti, D. F., et al. (2005), Unexpected changes to the global methane budget over the past 2000 years, *Science*, *309*(5741), 1714–1717, doi:10.1126/science.1115193.

Fischer, H., et al. (2008), Changing boreal methane sources and constant biomass burning during the last termination, *Nature*, *452*(7189), 864–867, doi:10.1038/nature06825.

Fogg, P. G. T., and J. Sangster (2003), *Chemicals in the Atmosphere: Solubility, Sources, and Reactivity*, 453 pp., John Wiley, Hoboken, N. J.

Forster, P., et al. (2007), Changes in atmospheric constituents and in radiative forcing, in *Climate Change 2007: The Physical Science Basis. Contribution of Working Group I to the Fourth Assessment Report of the Intergovernmental Panel on Climate Change*, edited by S. Solomon et al., pp. 131–234, Cambridge Univ. Press, Cambridge, U. K.

Grachev, A. M., E. J. Brook, and J. P. Severinghaus (2007), Abrupt changes in atmospheric methane at the MIS 5b-5a transition, *Geophys. Res. Lett.*, *34*, L20703, doi:10.1029/2007GL029799.

Grachev, A. M., E. J. Brook, J. P. Severinghaus, and N. G. Pisias (2009), Relative timing and variability of atmospheric methane and GISP2 oxygen isotopes between 68 and 86 ka, *Global Biogeochem. Cycles*, *23*, GB2009, doi:10.1029/2008GB003330.

Grudd, H., K. R. Briffa, W. Karlen, T. S. Bartholin, P. D. Jones, and B. Kromer (2002), A 7400-year tree-ring chronology in northern Swedish Lapland: Natural climatic variability expressed on annual to millennial timescales, *Holocene*, *12*(6), 657–665, doi:10.1191/0959683602hl578rp.

Gu, G. J., R. F. Adler, G. J. Huffman, and S. Curtis (2007), Tropical rainfall variability on interannual-to-interdecadal and longer time scales derived from the GPCP monthly product, *J. Clim.*, *20*(15), 4033–4046, doi:10.1175/JCLI4227.1.

Harder, S. L., D. T. Shindell, G. A. Schmidt, and E. J. Brook (2007), A global climate model study of CH_4 emissions during the Holocene and glacial-interglacial transitions constrained by ice core data, *Global Biogeochem. Cycles*, *21*, GB1011, doi:10.1029/2005GB002680.

Hegerl, G. C., T. J. Crowley, M. Allen, W. T. Hyde, H. N. Pollack, J. Smerdon, and E. Zorita (2007), Detection of human influence on a new, validated 1500-year temperature reconstruction, *J. Clim.*, *20*(4), 650–666, doi:10.1175/JCLI4011.1.

Houweling, S., F. Dentener, and J. Lelieveld (2000), Simulation of preindustrial atmospheric methane to constrain the global source strength of natural wetlands, *J. Geophys. Res.*, *105*(D13), 17,243–17,255, doi:10.1029/2000JD900193.

Houweling, S., G. R. van der Werf, K. K. Goldewijk, T. Rockmann, and I. Aben (2008), Early anthropogenic CH_4 emissions and the variation

of CH_4 and $^{13}CH_4$ over the last millennium, *Global Biogeochem. Cycles*, *22*, GB1002, doi:10.1029/2007GB002961.

Hu, C. Y., G. M. Henderson, J. H. Huang, S. Xie, Y. Sun, and K. R. Johnson (2008), Quantification of Holocene Asian monsoon rainfall from spatially separated cave records, *Earth Planet. Sci. Lett.*, *266*(3–4), 221–232, doi:10.1016/j.epsl.2007.10.015.

Huber, C., M. Leuenberger, R. Spahni, J. Fluckiger, J. Schwander, T. F. Stocker, S. Johnsen, A. Landals, and J. Jouzel (2006), Isotope calibrated Greenland temperature record over Marine Isotope Stage 3 and its relation to CH4, *Earth Planet. Sci. Lett.*, *243*(3–4), 504–519, doi:10.1016/j.epsl.2006.01.002.

Johnsen, S. J., et al. (1997), The $\delta^{18}O$ record along the Greenland Ice Core Project deep ice core and the problem of possible Eemian climatic instability, *J. Geophys. Res.*, *102*(C12), 26,397–26,410, doi:10.1029/97JC00167.

Jones, P. D., et al. (2009), High-resolution palaeoclimatology of the last millennium: A review of current status and future prospects, *Holocene*, *19*(1), 3–49, doi:10.1177/0959683608098952.

Kaplan, J. O., G. Folberth, and D. A. Hauglustaine (2006), Role of methane and biogenic volatile organic compound sources in late glacial and Holocene fluctuations of atmospheric methane concentrations, *Global Biogeochem. Cycles*, *20*, GB2016, doi:10.1029/2005GB002590.

Kaufman, D. S., D. P. Schneider, N. P. McKay, C. M. Ammann, R. S. Bradley, K. R. Briffa, G. H. Miller, B. L. Otto-Bliesner, J. T. Overpeck, and B. M. Vinther (2009), Recent warming reverses long-term arctic cooling, *Science*, *325*(5945), 1236–1239, doi:10.1126/science.1173983.

Khalil, M. A. K. (Ed.) (2000), *Atmospheric Methane: Its Role in the Global Environment*, 341 pp., Springer, Berlin.

Khalil, M. A. K., and R. A. Rasmussen (1983), Sources, sinks, and seasonal cycles of atmospheric methane, *J. Geophys. Res.*, *88*(C9), 5131–5144, doi:10.1029/JC088iC09p05131.

Kobashi, T., J. Severinghaus, J.-M. Barnola, K. Kawamura, T. Carter, and T. Nakaegawa (2010), Persistent multi-decadal Greenland temperature fluctuation through the last millennium, *Clim. Change*, *100*, 733–756, doi:10.1007/s10584-009-9689-9.

Lea, D. W., D. K. Pak, L. C. Peterson, and K. A. Hughen (2003), Synchroneity of tropical and high-latitude Atlantic temperatures over the last glacial termination, *Science*, *301*(5638), 1361–1364, doi:10.1126/science.1088470.

Lelieveld, J., P. J. Crutzen, and F. J. Dentener (1998), Changing concentration, lifetime and climate forcing of atmospheric methane, *Tellus, Ser. B*, *50*(2), 128–150, doi:10.1034/j.1600-0889.1998.t01-1-00002.x.

Lemieux-Dudon, B., E. Blayo, J. R. Petit, C. Waelbroeck, A. Svensson, C. Ritz, J. M. Barnola, B. M. Narcisi, and F. Parrenin (2010), Consistent dating for Antarctic and Greenland ice cores, *Quat. Sci. Rev.*, *29*(1–2), 8–20, doi:10.1016/j.quascirev.2009.11.010.

Loulergue, L., A. Schilt, R. Spahni, V. Masson-Delmotte, T. Blunier, B. Lemieux, J. M. Barnola, D. Raynaud, T. F. Stocker, and J. Chappellaz (2008), Orbital and millennial-scale features of atmospheric CH_4 over the past 800,000 years, *Nature*, *453*(7193), 383–386, doi:10.1038/nature06950.

MacDonald, G. M., and R. A. Case (2005), Variations in the Pacific Decadal Oscillation over the past millennium, *Geophys. Res. Lett.*, *32*, L08703, doi:10.1029/2005GL022478.

MacFarling Meure, C., D. Etheridge, C. Trudinger, P. Steele, R. Langenfelds, T. van Ommen, A. Smith, and J. Elkins (2006), Law Dome CO_2, CH_4 and N_2O ice core records extended to 2000 years BP, *Geophys. Res. Lett.*, *33*, L14810, doi:10.1029/2006GL026152.

Mann, M. E., Z. Zhang, M. K. Hughes, R. S. Bradley, S. K. Miller, S. Rutherford, and F. Ni (2008), Proxy-based reconstructions of hemispheric and global surface temperature variations over the past two millennia, *Proc. Natl. Acad. Sci. U. S. A.*, *105*(36), 13,252–13,257, doi:10.1073/pnas.0805721105.

Mann, M. E., Z. H. Zhang, S. Rutherford, R. S. Bradley, M. K. Hughes, D. Shindell, C. Ammann, G. Faluvegi, and F. B. Ni (2009), Global signatures and dynamical origins of the Little Ice Age and Medieval Climate Anomaly, *Science*, *326*(5957), 1256–1260, doi:10.1126/science.1177303.

Mantua, N. J., and S. R. Hare (2002), The Pacific decadal oscillation, *J. Oceanogr.*, *58*(1), 35–44, doi:10.1023/A:1015820616384.

Mantua, N. J., S. R. Hare, Y. Zhang, J. M. Wallace, and R. C. Francis (1997), A Pacific interdecadal climate oscillation with impacts on salmon production, *Bull. Am. Meteorol. Soc.*, *78*(6), 1069–1079, doi:10.1175/1520-0477(1997)078<1069:APICOW>2.0.CO;2.

Marlon, J. R., P. J. Bartlein, C. Carcaillet, D. G. Gavin, S. P. Harrison, P. E. Higuera, F. Joos, M. J. Power, and I. C. Prentice (2008), Climate and human influences on global biomass burning over the past two millennia, *Nat. Geosci.*, *1*(10), 697–702, doi:10.1038/ngeo313.

Martinerie, P., G. P. Brasseur, and C. Granier (1995), The chemical composition of ancient atmospheres: A model study constrained by ice core data, *J. Geophys. Res.*, *100*(D7), 14,291–14,304, doi:10.1029/95JD00826.

Matthews, E. (2000), Wetlands, in *Atmospheric Methane: Its Role in the Global Environment*, edited by M. A. K. Khalil, pp. 202–233, Springer, Berlin.

Matthews, J. A., and K. R. Briffa (2005), The 'Little Ice Age': Re-evaluation of an evolving concept, *Geogr. Ann., Ser. A*, *87*(1), 17–36, doi:10.1111/j.0435-3676.2005.00242.x.

McEvedy, C., and R. Jones (1978), *Atlas of World Population History*, 368 pp., Penguin, London.

Mischler, J. A., T. A. Sowers, R. B. Alley, M. Battle, J. R. McConnell, L. Mitchell, T. Popp, E. Sofen, and M. K. Spencer (2009), Carbon and hydrogen isotopic composition of methane over the last 1000 years, *Global Biogeochem. Cycles*, *23*, GB4024, doi:10.1029/2009GB003460.

Mitchell, L., and E. J. Brook (2009), New high-precision, high-resolution records of atmospheric methane from Greenland and Antarctic ice cores: 0–1800 A.D, *Eos Trans. AGU*, *90*(52), Fall Meet. Suppl., Abstract PP41B-1524.

Moberg, A., D. M. Sonechkin, K. Holmgren, N. M. Datsenko, and W. Karlen (2005), Highly variable Northern Hemisphere temperatures reconstructed from low- and high-resolution proxy data, *Nature*, *433*(7026), 613–617, doi:10.1038/nature03265.

Morse, D. L., D. D. Blankenship, E. D. Waddington, and T. A. Neumann (2002), A site for deep ice coring in West Antarctica: Results from aerogeophysical surveys and thermo-kinematic modeling, *Ann. Glaciol.*, *35*, 36–44.

Oppo, D. W., Y. Rosenthal, and B. K. Linsley (2009), 2,000-year-long temperature and hydrology reconstructions from the Indo-Pacific warm pool, *Nature*, *460*(7259), 1113–1116, doi:10.1038/nature08233.

Palmer, A. S., T. D. van Ommen, M. A. J. Curran, V. Morgan, J. M. Souney, and P. A. Mayewski (2001), High-precision dating of volcanic events (A.D. 1301–1995) using ice cores from Law Dome, Antarctica, *J. Geophys. Res.*, *106*, 28,089–28,095, doi:10.1029/2001JD000330.

Petrenko, V. V., et al. (2008), A novel method for obtaining very large ancient air samples from ablating glacial ice for analyses of methane radiocarbon, *J. Glaciol.*, *54*(185), 233–244, doi:10.3189/002214308784886135.

Pongratz, J., C. Reick, T. Raddatz, and M. Claussen (2008), A reconstruction of global agricultural areas and land cover for the last millennium, *Global Biogeochem. Cycles*, *22*, GB3018, doi:10.1029/2007GB003153.

Prinn, R. G., et al. (2001), Evidence for substantial variations of atmospheric hydroxyl radicals in the past two decades, *Science*, *292*(5523), 1882–1888, doi:10.1126/science.1058673.

Reuter, J., L. Stott, D. Khider, A. Sinha, H. Cheng, and R. L. Edwards (2009), A new perspective on the hydroclimate variability in northern South America during the Little Ice Age, *Geophys. Res. Lett.*, *36*, L21706, doi:10.1029/2009GL041051.

Ruddiman, W. F. (2003), The anthropogenic greenhouse era began thousands of years ago, *Clim. Change*, *61*(3), 261–293, doi:10.1023/B:CLIM.0000004577.17928.fa.

Ruddiman, W. F. (2007), The early anthropogenic hypothesis: Challenges and responses, *Rev. Geophys.*, *45*, RG4001, doi:10.1029/2006RG000207.

Schwander, J. (1989), The transformation of snow to ice and the occlusion of gases, in *The Environmental Record in Glaciers and Ice Sheets*, edited by H. Oeschger and C. C. Langway, pp. 53–67, John Wiley, Chichester, U. K.

Schwander, J., J.-M. Barnola, C. Andrié, M. Leuenberger, A. Ludin, D. Raynaud, and B. Stauffer (1993), The age of the air in the firn and the ice at Summit, Greenland, *J. Geophys. Res.*, *98*(D2), 2831–2838, doi:10.1029/92JD02383.

Schwander, J., T. Sowers, J.-M. Barnola, T. Blunier, A. Fuchs, and B. Malaizé (1997), Age scale of the air in the summit ice: Implication for glacial-interglacial temperature change, *J. Geophys. Res.*, *102*(D16), 19,483–19,493, doi:10.1029/97JD01309.

Severinghaus, J. P., and E. J. Brook (1999), Abrupt climate change at the end of the last glacial period inferred from trapped air in polar ice, *Science*, *286*(5441), 930–934, doi:10.1126/science.286.5441.930.

Severinghaus, J. P., T. Sowers, E. J. Brook, R. B. Alley, and M. L. Bender (1998), Timing of abrupt climate change at the end of the Younger Dryas interval from thermally fractionated gases in polar ice, *Nature*, *391*(6663), 141–146, doi:10.1038/34346.

Shindell, D. T., G. Faluvegi, and N. Bell (2003), Preindustrial-to-present-day radiative forcing by tropospheric ozone from improved simulations with the GISS chemistry-climate GCM, *Atmos. Chem. Phys.*, *3*, 1675–1702, doi:10.5194/acp-3-1675-2003.

Sowers, T., M. Bender, and D. Raynaud (1989), Elemental and isotopic composition of occluded O_2 and N_2 in polar ice, *J. Geophys. Res.*, *94*(D4), 5137–5150, doi:10.1029/JD094iD04p05137.

Sowers, T., M. Bender, D. Raynaud, and Y. S. Korotkevich (1992), $\delta^{15}N$ of N_2 in air trapped in polar ice: A tracer of gas transport in the firn and a possible constraint on ice age-gas age differences, *J. Geophys. Res.*, *97*(D14), 15,683–15,697, doi:10.1029/92JD01297.

Spahni, R., J. Schwander, J. Fluckiger, B. Stauffer, J. Chappellaz, and D. Raynaud (2003), The attenuation of fast atmospheric CH_4 variations recorded in polar ice cores, *Geophys. Res. Lett.*, *30*(11), 1571, doi:10.1029/2003GL017093.

Steele, L. P., P. J. Fraser, R. A. Rasmussen, M. A. K. Khalil, T. J. Conway, A. J. Crawford, R. H. Gammon, K. A. Masarie, and K. W. Thoning (1987), The global distribution of methane in the troposphere, *J. Atmos. Chem.*, *5*(2), 125–171, doi:10.1007/BF00048857.

Subak, S. (1994), Methane from the House of Tudor and the Ming Dynasty: Anthropogenic emissions in the sixteenth century, *Chemosphere*, *29*(5), 843–854, doi:10.1016/0045-6535(94)90157-0.

Thompson, A. M. (1992), The oxidizing capacity of the Earth's atmosphere: Probable past and future changes, *Science*, *256*(5060), 1157–1165, doi:10.1126/science.256.5060.1157.

Trenberth, K. E., and L. Smith (2005), The mass of the atmosphere: A constraint on global analyses, *J. Clim.*, *18*(6), 864–875, doi:10.1175/JCLI-3299.1.

Trouet, V., J. Esper, N. E. Graham, A. Baker, J. D. Scourse, and D. C. Frank (2009), Persistent positive North Atlantic oscillation mode dominated the Medieval Climate Anomaly, *Science*, *324*(5923), 78–80, doi:10.1126/science.1166349.

Trudinger, C. M., L. G. Enting, D. M. Etheridge, R. J. Francey, V. A. Levchenko, L. P. Steele, D. Raynaud, and L. Arnaud (1997), Modeling air movement and bubble trapping in firn, *J. Geophys. Res.*, *102*(D6), 6747–6763, doi:10.1029/96JD03382.

Valdes, P. J., D. J. Beerling, and C. E. Johnson (2005), The ice age methane budget, *Geophys. Res. Lett.*, *32*, L02704, doi:10.1029/2004GL021004.

van Hulzen, J. B., R. Segers, P. M. van Bodegom, and P. A. Leffelaar (1999), Temperature effects on soil methane production: An explanation for observed variability, *Soil Biol. Biochem.*, *31*(14), 1919–1929, doi:10.1016/S0038-0717(99)00109-1.

Vinther, B. M., et al. (2006), A synchronized dating of three Greenland ice cores throughout the Holocene, *J. Geophys. Res.*, *111*, D13102, doi:10.1029/2005JD006921.

Walter, B. P., M. Heimann, and E. Matthews (2001a), Modeling modern methane emissions from natural wetlands: 1. Model description and results, *J. Geophys. Res.*, *106*(D24), 34,189–34,206, doi:10.1029/2001JD900165.

Walter, B. P., M. Heimann, and E. Matthews (2001b), Modeling modern methane emissions from natural wetlands: 2. Interannual variations 1982–1993, *J. Geophys. Res.*, *106*(D24), 34,207–34,219, doi:10.1029/2001JD900164.

Wang, D. Q., Z. L. Chen, and S. Y. Xu (2009), Methane emission from Yangtze estuarine wetland, China, *J. Geophys. Res.*, *114*, G02011, doi:10.1029/2008JG000857.

Wang, X. F., A. S. Auler, R. L. Edwards, H. Cheng, E. Ito, and M. Solheid (2006), Interhemispheric anti-phasing of rainfall during the last glacial period, *Quat. Sci. Rev.*, *25*(23–24), 3391–3403, doi:10.1016/j.quascirev.2006.02.009.

Wang, Y. H., and D. J. Jacob (1998), Anthropogenic forcing on tropospheric ozone and OH since preindustrial times, *J. Geophys. Res.*, *103*(D23), 31,123–31,135, doi:10.1029/1998JD100004.

Wang, Y. J., H. Cheng, R. L. Edwards, Z. S. An, J. Y. Wu, C. C. Shen, and J. A. Dorale (2001), A high-resolution absolute-dated late Pleistocene monsoon record from Hulu Cave, China, *Science*, *294*(5550), 2345–2348, doi:10.1126/science.1064618.

Wang, Y. J., H. Cheng, R. L. Edwards, Y. Q. He, X. G. Kong, Z. S. An, J. Y. Wu, M. J. Kelly, C. A. Dykoski, and X. D. Li (2005), The Holocene Asian monsoon: Links to solar changes and North Atlantic climate, *Science*, *308*(5723), 854–857, doi:10.1126/science.1106296.

Weatherford, J. (2004), *Genghis Khan and the Making of the Modern World*, 1st ed., Crown, New York.

Worthy, D. E. J., I. Levin, F. Hopper, M. K. Ernst, and N. B. A. Trivett (2000), Evidence for a link between climate and northern wetland methane emissions, *J. Geophys. Res.*, *105*(D3), 4031–4038, doi:10.1029/1999JD901100.

Zhang, D. D., P. Brecke, H. F. Lee, Y. Q. He, and J. Zhang (2007), Global climate change, war, and population decline in recent human history, *Proc. Natl. Acad. Sci. U. S. A.*, *104*(49), 19,214–19,219, doi:10.1073/pnas.0703073104.

Zhang, P. Z., et al. (2008), A test of climate, Sun, and culture relationships from an 1810-year Chinese cave record, *Science*, *322*(5903), 940–942, doi:10.1126/science.1163965.

Zona, D., W. C. Oechel, J. Kochendorfer, K. T. Paw U, A. N. Salyuk, P. C. Olivas, S. F. Oberbauer, and D. A. Lipson (2009), Methane fluxes during the initiation of a large-scale water table manipulation experiment in the Alaskan Arctic tundra, *Global Biogeochem. Cycles*, *23*, GB2013, doi:10.1029/2009GB003487.

E. J. Brook and L. E. Mitchell, Department of Geosciences, Oregon State University, 104 Wilkinson Hall, Corvallis, OR 97331, USA. (mitchelo@geo.oregonstate.edu)

J. R. McConnell and K. Taylor, Desert Research Institute, Nevada System of Higher Education, 2215 Raggio Pkwy., Reno, NV 89512, USA.

T. Sowers, Earth and Environmental Systems Institute, Pennsylvania State University, 237 Deike Bldg., University Park, PA 16802, USA.